Schweizerische Eidgenossenschaft
Confédération suisse
Confederazione Svizzera
Confederaziun svizra

Swiss Confederation

Federal Department of Home Affairs FDHA
Federal Office of Meteorology and Climatology MeteoSwiss

Scientific Report MeteoSwiss No. 95

Quantifying the uncertainty of spatial precipitation analyses with radar-gauge observation ensembles

Raphaela Vogel

ISSN: 1422-1381

Scientific Report MeteoSwiss No. 95

Quantifying the uncertainty of spatial precipitation analyses with radar-gauge observation ensembles

Raphaela Vogel

Recommended citation:
Vogel, R.: 2013, Quantifying the uncertainty of spatial precipitation analyses with radar-gauge observation ensembles, *Scientific Report MeteoSwiss,* **95,** 80 pp.

Editor:
Federal Office of Meteorology and Climatology, MeteoSwiss, © 2013

MeteoSwiss
Krähbühlstrasse 58
CH-8044 Zürich
T +41 44 256 91 11
www.meteoschweiz.ch

Abstract

Sound quantitative precipitation estimates (QPE) are a key component of many hydrological and meteorological applications. The small-scale variability of precipitation and the limited coverage and accuracy of observations pose a major challenge to QPE precision. This study investigates a geostatistical method that combines radar and rain gauge data, to (a) generate best estimate precipitation fields and to (b) simulate ensembles of random precipitation fields that are consistent with the observations and represent the inherent analysis uncertainty. Daily precipitation data for 2008 covering the territory of Switzerland are used. Data transformation is applied to improve the compliance with model assumptions. The accuracy of the point estimates and the reliability of the probabilistic estimates from kriging with external drift are evaluated. A technical verification and plausibility experiments comparing the spatial uncertainty of the generated observation ensembles are performed.

A systematic application for the entire year 2008 shows the combination to improve both the accuracy of the best estimates and the representation of intense precipitation. Radar information is particularly beneficial in summer, for distinguishing wet and dry areas, and when the density of the gauge network is low. Greater improvement in both accuracy and reliability of the QPE can be achieved, however, with additional gauges from a denser network rather than with the additional radar information.

The technical implementation of the conditional simulation procedure is verified to be successful. Illustrative example cases show the ensemble members to represent the spatial variability of precipitation and to realize extremes beyond the range of the observations. Ensembles with 100 members are found to be sufficient to plausibly reproduce the spatial uncertainties. The increased density and improved technology of both the automatic rain gauge and radar network in the future render the combination very attractive for real-time applications. The results of the conditional simulation experiments bring to light considerable uncertainties regarding the distribution of true precipitation, especially at small scales. Observation ensembles are a promising way for describing these uncertainties quantitatively, and there are interesting prospects for using them to propagate uncertainties into concrete applications.

Contents

1 Introduction

Precise estimates of precipitation fields are very important in many applications such as hydrological forecasting (e.g., Zappa et al., 2008; Young et al., 2000; Viviroli et al., 2009) or numerical weather prediction (e.g., Leuenberger and Rossa, 2007). The increased availability of high-resolution quantitative precipitation estimates (QPE) fosters such applications. Nevertheless, the precision of the QPE is constrained by the small-scale spatial and temporal variability of precipitation and the limited coverage and accuracy of observational monitoring systems. In a country with complex topography like Switzerland, these limiting factors are particularly significant.

Many climatological applications in Switzerland nowadays use precipitation fields generated with an interpolation of rain gauge measurements. The most important advantage of the rain gauge measurements is their accuracy in absolute terms. Their spatial representativity, however, is limited. Should we gather all 440 rain gauges within Switzerland, the total area covered would amount to less than $10m^2$. Additional limitations of rain gauge observations are errors induced by wind or snowdrift, which affect the accuracy depending on the prevalent precipitation situation (e.g., Sevruk, 1985).

In applications with a real-time focus it is more common to use precipitation estimates from radar observations. MeteoSwiss runs three weather radars providing data of high spatial and temporal resolution. Unfortunately, the use of empirical relationships to convert the indirect measurement of hydrometeor backscatter into a precipitation rate, visibility problems, ground clutter and uncertainties about the vertical profile render the radar information inaccurate. Due to the mountainous topography of Switzerland, the estimation of precipitation from backscattering measurements is particularly difficult and requires complicated processing procedures (see e.g. Germann et al., 2006).

One possible way to cope with the presented limitations of precipitation measurements is increasing the station density and improving the measurement technology. This is currently done by MeteoSwiss for both the automatic rain gauge and the radar network. In 2013, the SwissMetNet (SMN) will include 134 automatic stations, compared to less than 80 in 2009 (MeteoSwiss, 2010). Furthermore, the existing radar network is currently being updated with state-of-the-art dual polarization technology and the set up of two more radars in the inner alpine regions of the Grisons and the Valais is planned (MeteoSwiss, 2012).

A complementary approach is to advance methods of data processing to use the information delivered by the existing networks in a more beneficial way. As outlined in the previous paragraphs, rain gauge and radar measurements have opposing strengths and weaknesses. The idea of combining information from the two different measurement platforms is appealing. Both the high resolution of radar and the accuracy of rain gauge measurements could thereby be exploited. Merging radar and rain gauge data has been an intense field of research for many years and

different combination methods have been suggested. The inclusion of radar information has been found to improve the skill of the QPE (e.g., Goudenhoofdt and Delobbe, 2009; Erdin, 2009; Schuurmans et al., 2007). Combination methods are based either on deterministic (e.g., DeGaetano and Wilks, 2008) or stochastic interpolation concepts, where stochastic methods have the advantage of delivering a probabilistic estimate (i.e. a best estimate and an uncertainty measure). A popular class of stochastic combination methods is constructed within the framework of geostatistics. Goudenhoofdt and Delobbe (2009) find that geostatistical approaches accounting for the spatial covariance structure of precipitation fields perform best. Widely used geostatistical methods in the radar-gauge merging context are ordinary kriging of radar errors, kriging with external drift, indicator kriging and co-kriging (e.g., Erdin, 2009; Haberlandt, 2007; Seo, 1998; Krajewski, 1987; Sideris et al., submitted). Although the exact implementation of the kriging technique differs between applications, kriging with external drift was demonstrated to be particularly flexible and promising when applied over mid-sized countries where the structure of radar errors is sufficiently homogenous (e.g., Goudenhoofdt and Delobbe, 2009; Erdin, 2009; Haberlandt, 2007; Keller, 2012).

MeteoSwiss is interested in an optimal method to estimate high resolution daily precipitation fields in near real-time. This places high demands on data availability. The automatic SMN network provides high quality rain gauge data in real-time but, with only about 130 stations, at very limited spatial density. A method using the SMN network in conjunction with real-time daily aggregates from radar has the potential to significantly improve the quality of QPE. If successful, such an implementation could replace existing daily QPE data products based on gauge or radar data only.

This report presents an implementation and extended evaluation of kriging with external drift at the daily time scale. This work is heavily based on previous developments by Erdin (2009) and Erdin et al. (2012). KED is used to estimate precipitation with rain gauge data from the SMN station network. The precision of the point estimates and the reliability of the probabilistic estimates are compared to single-sensor reference methods. Our most important research question is the following: what is the benefit of using aggregated radar fields to estimate daily precipitation fields from the SMN station network with KED? Further, we are interested in the influence of the station density on estimation quality. To answer the stipulated questions we perform a systematic application for an entire year.

In spite of the significant improvements realized with geostatistical combination methods, the residual uncertainty in estimated precipitation fields is still large. Kriging provides a best estimate, which is a smoothed representation of reality (e.g., Ekström et al., 2007; Goovaerts, 1997; Webster and Oliver, 2007). As kriging minimizes the local error variance, small values are typically overestimated and large values underestimated (Goovaerts, 1997). In other words, if we randomly select 100 values from a field obtained as best estimate from kriging and fit a variogram to them, the variance would be much smaller compared to the variance in the original data. A way to represent the inherent variability in the observations is to generate stochastic ensembles of precipitation fields by conditional simulation. Each ensemble member generated by conditional simulation corresponds to a possible realization of the unknown true precipitation field given the available observations and the spatial covariance structure. All these realizations are equally probable. The QPE from the fields of best estimates already have an associated variance giving a clue about the probability with which a critical precipitation amount is realized at a particular location. Yet, this kriging variance does not

indicate the probability that the mean over a specific area exceeds a critical amount. This joint probability can be evaluated with the simulated ensembles through an averaging of the probabilities over a specific area (Webster and Oliver, 2007). The spread of this average between the ensemble members can be interpreted as the uncertainty in the QPE.

There is growing interest in applying conditional simulation to quantify uncertainties in QPE. The methods applied and data used differ greatly among studies published. Some studies focus on the spatial covariance structure only (e.g., Frei et al., 2008; Ahrens and Jaun, 2007; Clark and Slater, 2006), while others also account for temporal correlation in the measurements (e.g., Germann et al., 2009; Ekström et al., 2007). Whilst in most of the previous studies the simulations are conditioned on rain gauge measurements (e.g., Frei et al., 2008; Ahrens and Jaun, 2007; Ekström et al, 2007; Clark and Slater, 2006), Germann et al. (2009) simulate precipitation fields based on radar data and use rain gauge measurements of the past only to quantify the radar error covariance structure. To test their hydrological performance, observation ensembles can be fed into a hydrological model. This yields a distribution of response values with a spread representing the sensitivity of runoff to uncertainty in the input observations (e.g., Germann et al., 2009; Zappa et al., 2008).

To our knowledge, conditional simulation has not been applied in the context of radar and rain gauge combination. Yet, Rakovec et al. (2012) and Clark and Slater (2006) point out the potential improvement of adding radar data to gauge based ensembles. The increased use of combined data products will fuel new applications where an explicit quantification of uncertainty is desirable. The development of a stochastic observation ensemble technique in a radar-gauge merging context will foster such applications and may provide interesting insight into the level of uncertainty reduction attributable to radar. This thesis presents the first results of applying conditional simulation to merged radar–gauge data and investigates the plausibility of generated observation ensembles. The comparison with ensembles simulated with a rain gauge only reference method allows to investigate the specific benefit of the additional radar information.

The thesis pursues two goals, each addressed separately with a methods and results section. First, systematic evaluation of KED performance on a daily time scale using observations of the SMN station network and the operational MeteoSwiss radar composite. Second, application of conditional simulation to merged radar-gauge data and investigation of the uncertainty structure reflected in the generated observation ensembles. The structure of this thesis is therefore as follows. The precipitation data used and the events studied are described in chapter 2. The methodological background of the systematic analysis of KED is provided in chapter 3. The corresponding results and their discussion follows in chapter 4 and is split into two parts; the sensitivity analysis of data transformation and the systematic application of KED on the daily time scale. Chapter 5 describes the fundamentals of conditional simulation and presents the implemented conditional simulation technique. The results and discussion section of conditional simulation is presented in chapter 6. We bring back together the narrative on KED and conditional simulation for the conclusions in chapter 7.

2 Data

2.1 Precipitation data

Daily aggregated precipitation data from rain gauges and radar over the domain of Switzerland are used in this study. The daily precipitation amount of both rain gauges and radar corresponds to the 24 hours sum from 06:00 UTC of a specific day to 06:00 UTC of the following day. All data used in this study is provided by MeteoSwiss.

2.1.1 Rain gauge data

Rain gauges are a widely used device to measure precipitation. A classical gauge consists of a barrel with 200 cm^2 collecting orifice. This study distinguishes two station networks with different densities, both operated by MeteoSwiss. The station network termed SMN incorporates observations from the 75 automatically measuring SwissMetNet (SMN) stations with 10 min time resolution operational in 2008. In addition to the SMN stations, the second station network ALL also includes the observations from the 366 climatological stations operated manually with daily time resolution. The distribution of the rain gauges is shown in Figure 1. The stations are evenly distributed over the whole domain. High-elevation areas, however, are underrepresented especially in the automatic SMN network. The data undergoes automatic and manual quality control prior to utilization (Scherrer et al., 2011). Since implausible observations are excluded from the analysis, the station base varies over time. Rain gauges are fairly accurate in absolute terms (Frei et al., 2008) and the rain gauge measurements are assumed to represent the correct values of precipitation at their respective locations.

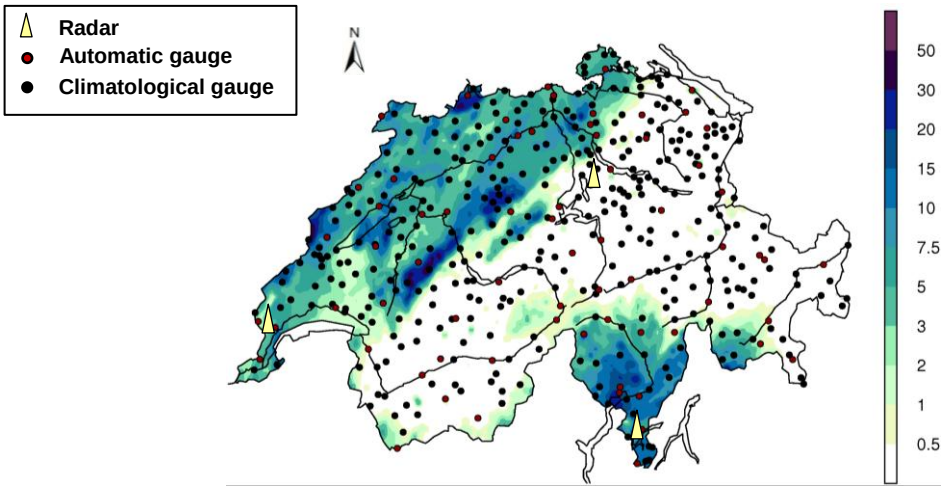

Figure 1 Radar composite of precipitation on the 16 May 2008 (mm per day). The radar locations at La Dôle, Monte Lema and Albis are marked in yellow. The circles indicate the locations of the rain gauges used in this study. The black circles represent the climatological and the red circles the automatic gauges. The station network referred to as ALL includes both the climatological and the automatic gauges, whereas SMN only includes the automatic SMN gauges.

2.1.2 Radar data

A weather radar is an active remote sensing instrument sending out electromagnetic wave pulses. The reflectivity of backscattered radiation by hydrometeors, R, is measured and turned into an estimate of the rain rate Z based on an empirical relationship of the form $Z=a*R^b$. At MeteoSwiss, the relation

$$Z = 316 \times R^{1.5}$$

is used (Germann et al., 2006). In 2008 - the period examined in this study - MeteoSwiss operated three C-band radars located in Central (Albis), Western (La Dôle) and Southern (Monte Lema) Switzerland (see Figure 2.1.1). We use composites from the three radars with a grid spacing of 1 km and a time resolution of one day, inferred by accumulation of 5-minute composites. We refer to Germann et al. (2006) for a detailed description of radar data processing implemented in Switzerland. The radar values at gauge locations are determined by nearest neighbor, i.e. by the radar value of the nearest grid point.

2.2 Studied events

Erdin et al. (2012) performed a systematic evaluation of KED for hourly precipitation over one year. Since they used the year 2008, this thesis also uses data from 2008 for the systematic application of KED to daily precipitation sums. This theoretically enables the comparison of estimation quality between the daily and hourly time scales.

The conditional simulation procedure applied in this thesis is a first exploratory step into a new field. We perform it as a case study and investigate three different precipitation events on the daily time scale (see Figure 2). We choose the 8 August 2007 as an example of stratiform precipitation due to intense precipitation fallen all over Switzerland. In the west, rain gauges and radar observations show a strong disagreement. The 10 June 2008 is characterized by isolated convective precipitation with intense fine-scale precipitation cells present. Radar and rain gauge measurements are agreeing well. Overall convective precipitation was encountered on the 6 September 2008. Precipitation is abundant all over the domain, with a distinct maximum in the Ticino.

In addition, monthly aggregates from daily precipitation for the three months of January, May and July 2008 are studied.

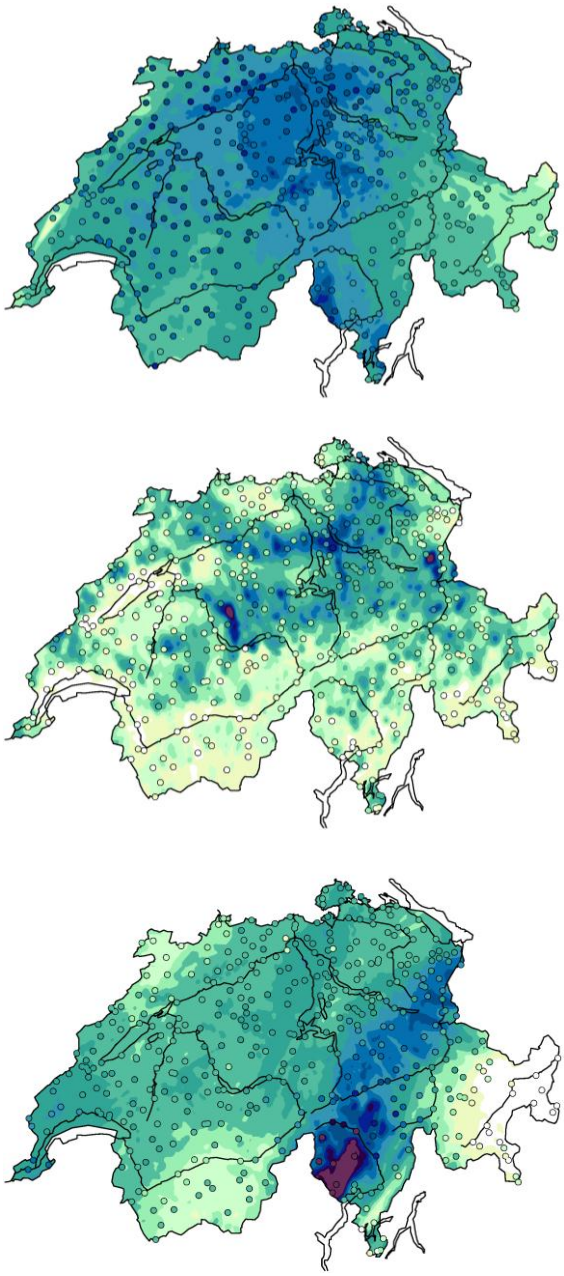

08 August 2007

Stratiform precipitation

Combination (KED/CSCOMB):

β_{smn} = 0.368, β_{all} = 0.335

λ_{smn} = 0.523, λ_{all} = 0.602

Single-sensor reference (OKGAU/CSGAU):

λ_{smn} = 0.62, λ_{all} = 0.715

10 June 2008

Isolated convective precipitation

Combination (KED/CSCOMB):

β_{smn} = 0.938, β_{all} = 0.888

λ_{smn} = 0.26, λ_{all} = 0.309

Single-sensor reference (OKGAU/CSGAU):

λ_{smn} = 0.266, λ_{all} = 0.275

06 September 2008

Overall convective precipitation

Combination (KED/CSCOMB):

β_{smn} = 0.777, β_{all} = 0.675

λ_{smn} = 0.302, λ_{all} = 0.341

Single-sensor reference (OKGAU/CSGAU):

λ_{smn} = 0.358, λ_{all} = 0.365

Figure 2 Radar composite and rain gauge measurements of the three example days investigated in the case study of conditional simulation. For every example day the characteristic precipitation situation is indicated. The value of the transformation parameter λ (see section 3.3 for a description of data transformation) is given for the combination (KED and CSCOMB) and the single-sensor reference (OKGAU and CSGAU) for both station networks. The radar coefficients β (from equation 1, section 3.2) are provided for the combination with both station networks. More information on the parameters, the combination and the reference method follow in section 3 and 5. Values are given in mm with the same scale for every image.

3 Methods radar-gauge combination

The theoretical background of the systematic evaluation of daily precipitation fields estimated with KED is provided in this chapter. Section 1 presents the fundamentals of geostatistics. The second section is dedicated to the specific radar-gauge combination used. The applied data transformation is discussed in section 3. A detailed description of the evaluation technique is provided in section 4. In Section 5 follows a specification of the software used.

3.1 Geostatistics

Geostatistics uses spatially referenced data from a continuous varying field to provide estimates of a variable wherever desired. In the following, the basic principles of geostatistics are discussed. For more detailed information readers are referred to Cressie (1993), Goovaerts (1997) or Webster and Oliver (2007).

In geostatistics, precipitation at a certain point in space is interpreted as a realization of a multivariate random variable. The characteristics of this random variable can be described by a parametric model. Such a stochastic concept is helpful since information on the deterministic processes causing the variability of precipitation is limited. The available precipitation observations are perceived as one realization of this multivariate random variable. The underlying model decomposes the random process in a deterministic and a stochastic component. The deterministic component (trend) corresponds to a first approximation of the field and can be a constant value or a linear model similar to a linear regression. The stochastic component describes the spatial covariance structure of the deviations from this trend field (the random process).

Modeling the random process necessitates two assumptions. First, we assume the random process to be of Gaussian distribution in some transformed space (see later). Second, we have to make stationarity assumptions. Since observations are sparse with regard to the large domain, we assume the random process to have certain attributes that are the same everywhere. The concept of weak stationarity is used here. Weak stationarity assumes the expected value and the variance of the Gaussian distribution to be constant and the covariance to depend only on the lag distance between two points (rather than on their absolute position).

The random process is modeled with a parametric semivariogram model. Figure 3 shows such a variogram for the 10 June 2008. It manifests what is intuitively clear: The variance between observations increases with increasing lag distance. The fit of an exponential variogram function to the data requires the estimation of the variogram parameters *nugget*, a measure of spatially unstructured variation, *sill*, the variance of the stochastic process and *range*, the maximum distance over which observations are correlated.

Kriging is the geostatistical estimation method corresponding to the stochastic model just outlined. By kriging we can produce a best estimate of precipitation and a measure of its uncertainty (i.e. the kriging variance) for every location in the domain. The estimates are weighted linear combinations of the data, with weights determined by the variogram. Kriging is optimal in the sense that it produces

unbiased estimates and minimizes the estimation errors. The following section describes the specific kriging technique applied.

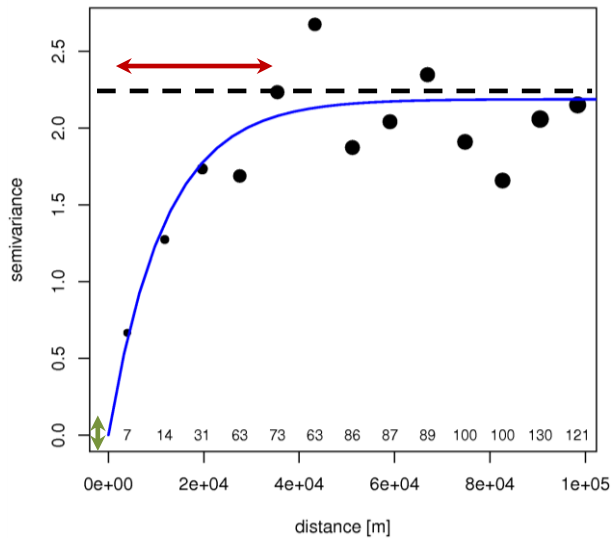

Figure 3 Example variogram from KED with the sparse SMN station network for 10 June 2008. The black dots represent the semivariances of the binned empirical variogram. The dot size and the small numbers above the x-axis show the number of observed pairs in the specific bins. The fitted exponential variogram function is shown in blue. The variogram parameters partial sill (dashed black line) is 2.2, the range (red arrow) is 35 km and the nugget (green arrow) is zero.

3.2 Kriging with external drift

KED is a popular kriging technique in the radar–gauge merging context (e.g., Erdin et al., 2012; Haberlandt 2007; Schuurmans, 2007; Goudenhoofdt and Delobbe, 2009). The deterministic component (i.e. trend or drift) of KED is based on external data. We use radar information for this external drift. The KED technique used here was implemented by Erdin (2009) and refined by Erdin et al. (2012).

The precipitation amount P (in some transformed space, see later) on the target grid with indices i and j and a resolution of 1 km^2 is modeled as follows:

$$P_{i,j} = \underbrace{\alpha + \beta \cdot \mathrm{Radar}_{i,j}}_{\text{Trend; deterministic part}} + \underbrace{Z_{i,j}}_{\text{Random process; stochastic part}} \qquad (1)$$

where α and β are the intercept and the radar coefficient of the deterministic part. $\mathrm{Radar}_{i,j}$ is the radar value at the given grid point and Z refers to a random process representing the multivariate Gaussian random variable of the residuals (i.e. the deviation of gauge observations from the trend).

All the model parameters are estimated jointly by maximum likelihood estimation (MLE) for every studied day. Since it accounts for the limited sample size, we use the method of restricted MLE (REML) for parameter estimation. An exponential model is used for variogram fitting. As the sample size for variogram fitting is small, we use an isotropic variogram, i.e. assume the same spatial

correlation in all the directions. In order to guarantee robust parameter estimation, we only analyze days with at least ten wet (≥ 0.5 mm per day) SMN stations.

3.3 Data transformation

Precipitation data is non-negative and skewed and therefore deviates from normality. The stochastic model of geostatistics, however, assumes a Gaussian distribution This violation of model assumptions can be reduced with appropriate data transformation prior to the application of kriging. One of the frequently used transformations was proposed by Box and Cox (1964). It has the following form:

$$Y^* = \begin{cases} \frac{Y^\lambda - 1}{\lambda} & \lambda \neq 0 \\ \log(Y) & \lambda = 0 \end{cases}$$

with Y* and Y denoting the transformed and untransformed precipitation data. λ serves as the transformation parameter. KED is performed on the transformed scale and transformation is applied to both radar and rain gauge observations. The results in transformed space are finally back-transformed into precipitation space by inverse application of the Box-Cox transformation.

Erdin et al. (2012) studied the influence of data transformation on estimation quality. They find a case-dependent λ to be the most appropriate choice. We follow this recommendation and estimate case-dependent λs with MLE for every day and station density specifically. Since excessive transformation can introduce a positive bias (Erdin et al., 2012), we apply a lower bound to the estimation of λ with a prior distribution. Section 4.1 provides the results of the sensitivity analysis for the most appropriate choice of this lower bound. Model diagnostics show that the applied transformation leads to good compliance with the model assumptions (not shown here).

3.4 Evaluation

In order to assess the performance of KED, we perform an extended evaluation of the quality of the QPE. Cross validation is the basis for further analysis and explained in the first subsection. The next subsection presents the skill measures compared. In the third subsection, we present how the cross-validated probabilistic estimates can be used to investigate the reliability of the probabilistic estimates, i.e. whether the kriging variance describes uncertainties appropriately. Single-sensor reference methods used to quantify a potential benefit of the combination are described in subsection 4.

3.4.1 Cross validation

Cross validation is a common technique to assess the skill of spatial interpolation methods and often applied with radar-gauge combinations (e.g., Haberlandt, 2007; Clark and Slater, 2006). Thereby, the precipitation amount at a certain gauge location is estimated with a model fitted to the data without using the measurement at the specific gauge itself. These estimations are then compared to the observations and the so called cross validation errors are computed from the difference between observed and estimated values. This procedure is repeated for all the observations successively.

We use cross validation at all gauges for precipitation fields estimated with the dense station network ALL. When using KED with the SMN station network, we perform a test data validation with the climatological gauges besides the cross validation at SMN stations. The observations at the climatological gauges were not used for the model estimation and serve as independent set of test data. The observations at these test locations are compared to the model estimates to yield the estimation errors from test data validation. For further analysis, cross validation errors and estimation errors from test data validation are taken together. We have, thus, a complete set of validated estimates for both station networks. This is important for comparability and guarantees consistency.

3.4.2 Skill measures

The estimation errors from cross and test data validation can be condensed into a variety of skill measures. Since the different skill measures assess different abilities of a method, it is important not to rely on one skill measure only, but rather consider a number of different measures. Skill measures are calculated on a transformed scale to mitigate the predominance of errors at locations with intense precipitation. We either apply a square root (where not stated differently) or a logarithmic transformation to both observations and estimations. The transformation can reduce but not remove the problem that the estimation quality depends critically on the fallen precipitation amounts. Still, different precipitation situations are hardly comparable. The skill measures used are described extensively in Erdin (2011) and Keller (2012). A brief description is provided in the following.

The skill measure *Bias* assesses systematic errors of a method and is computed on logarithmic scale (in dB). The best measure of the Bias is 0 dB. Negative (positive) values of the Bias refer to an underestimation (overestimation) of precipitation.

$$Bias = 10\ \log_{10}\left(\frac{\sum_i\ est}{\sum_i\ obs}\right)$$

The *relative mean root transformed error* (Rel. MRTE) is a measure of overall quality of a method. It is the MRTE normalized by the mean root transformed deviation (MRTD). For the Rel. MRTE, the best measure is 0.

$$Rel.MRTE = \frac{\mathrm{MRTE}}{MRTD} = \left(\frac{\frac{1}{n}\sum_{i=1}^{n}\left(\sqrt{est_i} - \sqrt{obs_i}\right)^2}{\frac{1}{n}\sum_{i=1}^{n}\left(\sqrt{obs_i} - \sqrt{\overline{obs}}\right)^2}\right)$$

Whether a method distinguishes well between wet and dry areas is evaluated with the *Hanssen-Kuipers discriminant* (HK). The false alarm ratio (number of wet estimations when observations were dry, divided by the number of all dry events) is subtracted from the probability of detection (correctly estimated wet events divided by all the observed wet events) to yield the HK (see Wilks (2006) for details). Whilst a perfect estimation has a HK of 1, a HK of 0 implies no additional skill of the estimation over a random estimation.

SCATTER assesses the performance of a method to quantify precipitation in areas where precipitation is estimated and observed. Proposed by Germann et al. (2006), the skill measure is defined as half the distance between the 16% and the 84% quantiles of the cumulative error

distribution function (CEDF; the cumulative contribution to total precipitation as a function of the radar-gauge ratio on days where both estimation and observation are wet). A SCATTER of 0 dB signifies best performance.

$$SCATTER = \frac{1}{2}\ (CEDF_{84} - CEDF_{16})$$

The *stable equitable error in probability space* (SEEPS) is a three category error measure. It assesses the ability of a method to distinguish between dry, light (defined as the lower two thirds of all wet observations) and intense (upper third) precipitation. More Information on SEEPS is supplied in Rodwell et al. (2010). The best measure of the SEEPS is 0.

The *median absolute deviation* (MAD) is, as the Rel. MRTE, a measure assessing the overall quality of a method. Yet, it is less influenced by outliers. A MAD of 0 refers to an error-free estimation.

$$MAD = \text{median}\left(\left|\sqrt{est} - \sqrt{obs}\right|\right)$$

3.4.3 Reliability of the probabilistic estimates

The reliability of the QPE is assessed by comparing the gauge measurements with the probability density function (pdf) of the corresponding cross-validated probabilistic estimate. For a probabilistic forecast (i.e. a probabilistic prediction in space), reliability refers to the statistical consistency between estimated probabilities and observed relative frequencies (Wilks, 2006). In a fully reliable system, we would expect the frequency of gauge measurements smaller than quantile Q_p of its pertinent cross-validated probabilistic estimate to be *p*. We can compare the observed frequencies of measurements to fall into predefined interquantile bins of the probabilistic estimates to the expected frequencies in a fully reliable system. This provides information on the reliability of the kriging estimations. This reliability assessment is similar to the Talagrand diagram (Talagrand et al., 1997).

3.4.4 Reference methods for comparison

In this thesis we compare the estimation quality of KED to three single-sensor reference methods. They help to illustrate and quantify potential improvements achieved by combining radar and rain gauge data with KED. The reference methods used are ordinary kriging of gauges (OKGAU), a deterministic spatial interpolation (RHIRES), and a QPE product from radar (RADAR). OKGAU and RHIRES use information from rain gauges and RADAR uses radar information only.

OKGAU performs an ordinary kriging of gauge measurements. Since ordinary kriging is a geostatistical kriging technique, OKGAU has a deterministic and a stochastic part comparable to KED. In contrast to KED, however, the trend field in OKGAU is a constant (i.e. the mean of the gauge observations). Information on the spatial covariance structure of the deviations of gauge observations from the mean are added. OKGAU also supplies the kriging variance and allows evaluating the reliability of the estimates. Transformation, variogram modeling and parameter estimation are performed as for KED.

Data from all the automatic and climatological gauges are used in RHIRES. The analysis consists of an angular distance weighting scheme in combination with a local regression analysis. Details can be found in Frei and Schär (1998) and Frei et al. (2006). Here, RHIRES is used as a reference for comparing aggregated yearly precipitation.

Fields estimated with RADAR correspond to the radar composites also used for KED. We refer to the data section 2.1.2 and Germann et al. (2006) for a more detailed description of this radar product. The radar data supplied by MeteoSwiss are on the target grid already and need no further interpolation.

For ease of understanding, the different methods are designated hereafter in the following way: KED_all and KED_smn refer to the precipitation field estimated with the radar-gauge combination method KED and the station networks ALL and SMN. Estimations with OKGAU are called OKGAU_all and OKGAU_smn respectively. The two other reference methods are simply called RHIRES and RADAR.

3.5 Software

We use the free statistical software R, version 2.14.0 (R Development Core Team, 2011), for all the statistical analysis, plots and calculations performed. The geostatistical methods applied are based on the R-package geoR (Ribieiro and Diggle, 2001).

4 Radar-gauge merging at the daily time scale

We present and discuss the results of applying KED to estimate daily precipitation in this chapter. As motivated in the method section, we dedicate a first section to the analysis of the sensitivity of estimation quality on data transformation. In section 2 we show the results of the systematic application of KED for the entire year 2008.

4.1 Sensitivity analysis of data transformation

The importance of transformation to precipitation data was pointed out in section 3.1. Yet, Erdin et al. (2012) show that excessive transformation can result in a positive bias in the QPE. They find that 'as a consequence of the excessive skewness and precipitation dependence', experiments with prescribed λs lower than 0.2 resulted in such positive biases. The introduction of a lower bound to the transformation parameter λ was recommended. The lower bound could be implemented in the form of a prior distribution that operates as a constraint to the MLE of λ to avoid excessive transformation. On the hourly time scale, λ=0.2 was suggested as a sensible choice for this lower bound (Erdin et al., 2012).

Whether this setting of a lower bound of λ (λ_{lower}) should be adopted for the daily time scale requires a careful sensitivity analysis. On the one hand, we want a λ_{lower} such that excessive transformation is prevented. On the other hand, this lower bound should be low enough to allow MLE to find the most suitable λ for the given data. Hence, we perform cross validation to examine the accuracy of the point estimates and the reliability of the probabilistic estimates of different λ_{lower}.

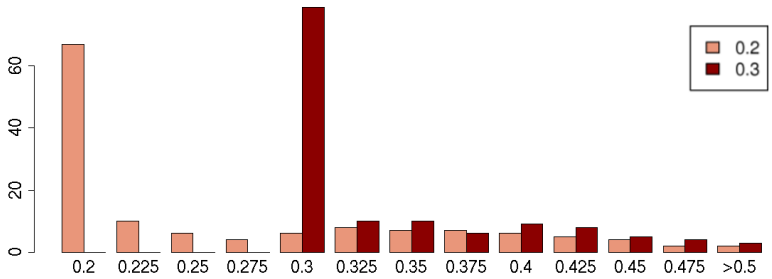

Figure 4 Histogram of the estimated transformation parameters λ from MLE for the two settings of λ_{lower} (λ_{lower} =0.2 and λ_{lower} =0.3). The realized values of λ (x-axis) are plotted against the number of days (y-axis) the specific λs were estimated. The label on the x-axis indicates the lower bound of the respective bin.

For this sensitivity analysis, we use a test period of 134 days in the six months of January, May, June, July, August and September of the year 2008. Considered are days when more than ten gauges registered precipitation. The fields are estimated with KED_all that serves as illustration example. We investigate the sensitivity of estimation quality to λ_{lower} with two different settings, λ_{lower} fixed at 0.2 and 0.3. The selection is motivated by the fact that λ_{lower} =0.2 proved to be the most successful choice for hourly precipitation. As the skewness of daily precipitation is expected to

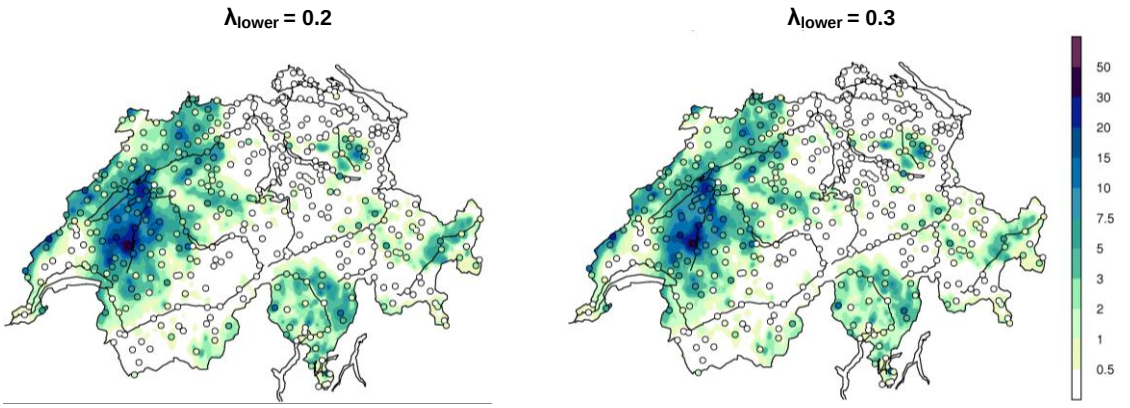

Figure 5 Best estimate fields of precipitation for the 11 May 2008 with KED_all for the two settings of λ_{lower} (λ_{lower} =0.2 and λ_{lower} =0.3). Realized λs are 0.22 (with λ_{lower}= 0.2) and 0.31 (with λ_{lower}=0.3). The filled circles represent the rain gauge measurements.

breduced compared to hourly precipitation, the λs realized on daily time scales will likely be higher and probably need a higher lower bound. Thus, we compare the impact of λ_{lower} =0.2 on estimation quality to the one with λ_{lower} =0.3.

We first turn towards the realized λs, i.e. the λs that were estimated by MLE given the constraint of the two different lower bounds (see Figure 4). For both λ_{lower}, the majority of estimated λs are close to the lower bound. The number of λs in the lowest bin increases for λ_{lower} =0.3, as it also includes many of the λs that fell into bins between 0.225 and 0.3 in the case of λ_{lower} =0.2. Yet, the λs estimated with λ_{lower} =0.3 tend to be higher also well above the threshold of 0.3. Whilst only on 19 days a λ exceeding 0.4 is estimated with λ_{lower} = 0.2, this figure goes up to 29 for λ_{lower} =0.3. We therefore argue that the choice of λ_{lower} really influences the MLE of λ.

Figure 5 shows the estimated fields of precipitation on the 11 May 2008 with the two different settings of λ_{lower}. Indeed, the case is representative for the experience that the best estimates are generally very similar between the two settings of λ_{lower}.

As the estimated fields do not reveal much about the quality of the estimation, we compare the skill measures of the two settings. The differences in skill between the two λ_{lower} for the complete sample of 134 estimated days are negligible (see Table 1). We do not find a positive bias for λ_{lower} =0.2. The Bias is rather less negative and even smaller in absolute terms compared to λ_{lower} =0.3.

Table 1: Skill measures Bias, Rel. MRTE, HK, SCATTER and SEEPS from systematic cross validation of KED_all for the two settings of λ_{lower} (λ_{lower}=0.2 and λ_{lower}=0.3). Skill measures are calculated from the pooled results of the 134 days of the test period.

	Bias (dB)	Rel. MRTE	HK	SCATTER (dB)	SEEPS
0.2	-0.01	0.10	0.84	1.32	0.17
0.3	-0.06	0.10	0.84	1.31	0.17

A certain difference in estimation quality between the two settings is evident in the probabilistic estimates. Figure 6 shows the relative frequencies with which measured precipitation falls into the predefined interquantile bins of the pertinent cross-validated probabilistic estimates. Frequencies are expressed relative to a fully reliable system. In a fully reliable system, we would for example expect 25% of the measurements to fall between the 25% and the 50% quantile. Thus, we divide the observed frequencies by these expected frequencies. A fully reliable system results in a straight line at 1.

For both λ_{lower}, the curves show the typical W-shape also observed for OKGAU and with the sparse station network (a more detailed discussion follows in section 4.2). Except for the lowest interquantile bin (below the 0.5% quantile), λ_{lower} =0.3 has relative frequencies closer to 1 and is therefore more reliable in the lower quantiles. In the upper quantiles, however, a lower bound of 0.2 produces more reliable estimates. In the uppermost interquantile bin (above the 99.5% quantile), the observed frequency for both λ_{lower} is three times higher than the expected. This indicates that very large point observations are considered as too unlikely by the uncertainty range estimated by KED.

We have another important option to analyze the impact of λ_{lower} on the quality of the QPE, namely to check how well intense precipitation is represented in the estimation of the precipitation fields. Table 2 shows the observed frequencies of measured intense precipitation to fall above the 99.5% quantile of its pertinent cross-validated probabilistic estimates. In these cases, the probabilistic estimate considers the observed precipitation as extremely unlikely. The frequency of extreme unlikeliness is desired to be small. As we look at intense precipitation only, we cannot compare it to the expected frequency of 0.5% a fully reliable system would exert when considering precipitation of all intensities. As an example for λ_{lower}=0.2, of all 9730 events a rain gauge registered precipitation above 10 mm, 220 (i.e. 2.26%) are classified as extremely unlikely by the pertinent cross-validated probabilistic estimate.

Overall, the percentage of intense precipitation classified as extremely unlikely by the probabilistic estimate is lower for λ_{lower} =0.2. Especially in the light of the conditional simulations that will be performed based on KED, a good representation of intense precipitation is important. Thus, λ_{lower}=0.2

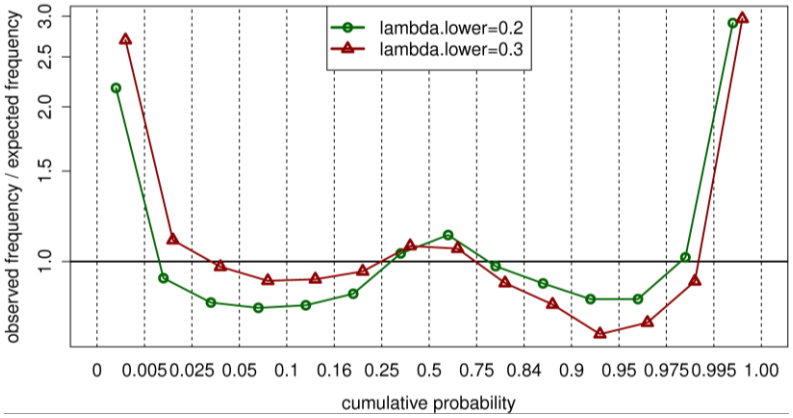

Figure 6 Frequency of gauge measurements to fall in interquantile bins of the pertinent cross-validated probabilistic estimate (x-axis). Frequencies are expressed relative to the expected frequency in a perfectly reliable system on log scale (y-axis). The bins of the distribution are defined by the 0.5%, 2.5%, 5%, 10%, 16%, 25%, 50%, 75%, 84%, 90%, 95%, 97.5%, 99.5% quantiles (dashed vertical lines). Shown are results from KED_all for the 134 days of the test period with the two settings of the lower bound to lambda, λ_{lower} =0.2 and λ_{lower} =0.3.

has an advantage here. The skill measures (here the Bias, the Rel. MRTE and the MAD; see Table 2) for intense precipitation exceeding predefined thresholds are similar for both settings of λ_{lower}.

To summarize, the different λ_{lower} do not influence the quality of the best estimates. Yet, some advantages of λ_{lower} =0.2 can be made out when comparing the probabilistic estimates. Coming back to the dilemma mentioned in the beginning, we see that we do not have the disadvantage of a positive bias with the lower λ_{lower}. Moreover, the advantages of a less constrained MLE and better representation of intense precipitation clearly favor the choice of 0.2 as λ_{lower}. The choice of the lower bound to λ is therefore 0.2 for our daily application and hence the same as proposed for the hourly time scale.

This sensitivity analysis was carried out with the geostatistical method of KED using rain gauge observations from the dense station network ALL. We expect the sensitivity of estimation quality to data transformation not to be influenced by the number of stations used. Figure 8 of the following section shows a histogram of the realized λs of KED and OKGAU. No major differences between the two can be made out. We therefore stick to the choice of λ_{lower} =0.2 also for OKGAU and in applications with the SMN network.

Table 2: Percentage of measured intense precipitation events classified as extremely unlikely (corresponding to the exceedance of the 99.5% quantile) by the pertinent cross validated probabilistic estimate for the two settings of λ_{lower} (λ_{lower}=0.2 and λ_{lower}=0.3). Intense precipitation refers to the exceedance of the predefined thresholds of 10, 20, 40 and 80 mm. The number of events where measurements exceeded these thresholds is listed. The skill measures Bias, Rel. MRTE and MAD are shown for precipitation exceeding the above thresholds. Error measures and percentages are calculated from KED_all for the 134 days of the test period.

Threshold	No. of events	Observed frequency in the 99.5% quantile		Bias (dB)		Rel. MRTE		MAD	
		0.2	0.3	0.2	0.3	0.2	0.3	0.2	0.3
10 mm	9730	2.26%	2.83%	-0.32	-0.36	0.37	0.37	3.34	3.34
20 mm	4252	2.99%	3.60%	-0.42	-0.44	0.54	0.54	4.73	4.73
40 mm	1032	4.94%	5.14%	-0.50	-0.51	0.74	0.74	6.70	6.70
80 mm	104	10.58%	12.50%	-0.70	-0.69	1.08	1.04	18.63	18.78

4.2 Systematic evaluation of KED for daily precipitation

Equipped with a carefully chosen λ_{lower}, we now turn towards the systematic evaluation of KED. The systematic analysis of the year 2008 encompasses 218 day where both station densities (SMN and ALL) registered at least ten wet (≥ 0.5 mm per day) gauges. This constraint is set to avoid robustness problems in case of very few wet gauges.

In the following we first have a look at the QPE of an example day. Subsection 2 then discusses the estimated model parameters. The accuracy of the point estimates is investigated in subsection 3. A fourth subsection is dedicated to analyzing the reliability of the probabilistic estimates. Intense precipitation is treated in the following subsection 5. The last subsection focuses on the annual distribution of precipitation.

4.2.1 Example case

Before we start discussing the systematic application of KED for the year 2008, let us have a qualitative look at the precipitation distribution of a single day. The estimated precipitation fields from KED and the single-sensor references for both station densities are shown in Figure 7 for the 10 June 2008. This example case is characteristic for an intense convective isolated precipitation situation with several isolated, small-scale and slow moving precipitation cells (see also Figure 2). The filled circles in Figure 7 show the rain gauge observations. If the field is estimated with SMN stations only, the SMN stations are framed with red. As they allow for an interesting comparison of the best estimates with the gauge observations, the climatological stations are still plotted.

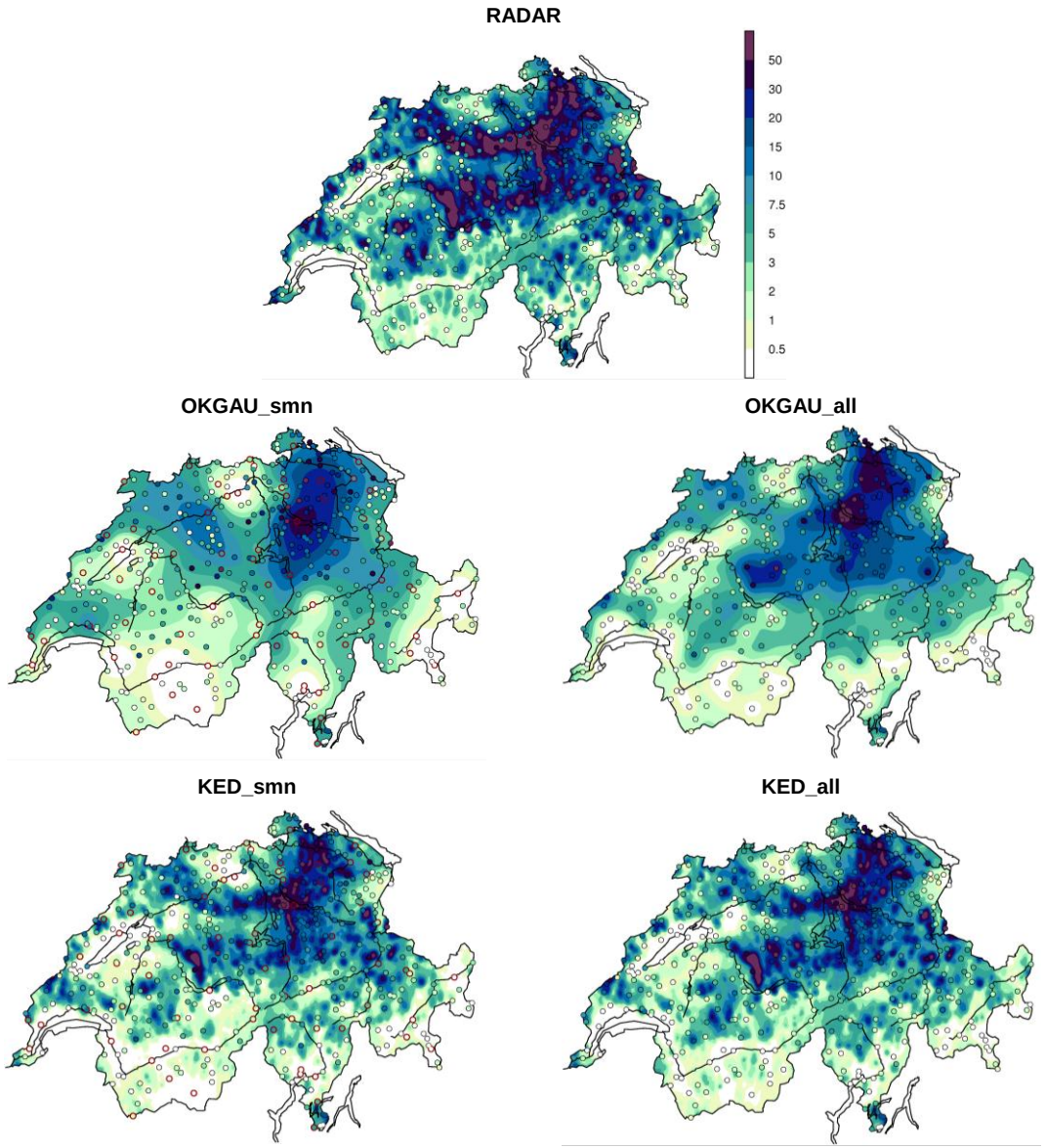

Figure 7 Estimated fields of precipitation (in mm) for the 10 June 2008 with RADAR, OKGAU_smn, OKGAU_all, KED_smn and KED_all. The filled circles represent the rain gauge measurements. For OKGAU_smn and KED_smn, the SMN stations are highlighted in red.

In the RADAR field, precipitation is clearly overestimated. This is particularly visible close to rain gauge locations, where the RADAR field often deviates from the gauge measurements. We understand these deviations as the low accuracy of radar information when it comes to point estimation. The fine-scale precipitation patterns, however, are well represented in the RADAR field.

Also for this day with presumably high spatial variability of precipitation (as manifested in the RADAR field), precipitation fields from OKGAU are very smooth. Although OKGAU is able to represent the overall features of the precipitation distribution, the loss of information about the unknown true field is potentially big. The low skill of the estimation is particularly evident for OKGAU_smn. The estimated field does not match the observations at climatological gauges at all. Information on the fine-scale precipitation pattern is clearly lacking.

In the combined QPE, we find a good representation of the fine-scale precipitation pattern. The high radar coefficients (β_{KED_all}= 0.89, β_{KED_smn} = 0.94; see Figure 2) indicate, after correction of the systematic overestimation, a lot of agreement between radar and gauge observations. Intense precipitation observed by the radar is therefore well-represented also in regions between the rain gauges, and the systematic bias of the radar information is corrected. When radar information is included, the smaller station network does not seem to lower the quality of the estimated field too much. The estimated field of KED_smn at climatological gauges (i.e. gauges that were not used to estimate the model with) compare well with the observations.

This example case suggests that adding radar information to rain gauge measurements is particularly beneficial in convective situations with high spatial variability of precipitation. This hypothesis will be supported in the following systematic analysis.

4.2.2 Estimated parameters

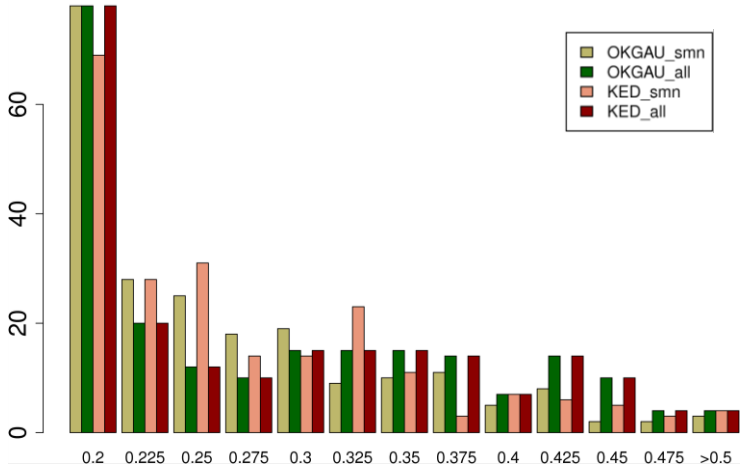

Figure 8 Histogram of the estimated transformation parameters λ with OKGAU_smn, OKGAU_all, KED_smn and KED_all for the 218 estimated days of 2008. The realized values of λ (x-axis) are plotted against the number of days (y-axis) the specific λs were estimated. The label on the x-axis indicates the lower bound of the respective bin.

The transformation parameters λ estimated with MLE are shown in Figure 8 for KED and OKGAU with both station densities. On 60 to 80 days, the λs fall close to the lower bound of 0.2. All methods show a similar distribution of the frequencies of realized λs. For KED_smn, however, higher values of λ are more frequently realized.

Figure 9 compares the radar trend coefficient β (from equation (1)) estimated by KED with both station densities. The correlation between the two estimates is positive, i.e. the estimates are jointly adjusted with respect to the agreement of radar and gauge observations at gauge locations. The βs estimated with KED_smn, however, are systematically larger (i.e. off the 1:1 line). The mean values of the βs (β_{mean,KED_all} =0.43, $\beta_{mean,\ KED\_smn}$ =0.59) differ by 0.16. A Student's t-test of this difference is highly significant with a p-value smaller than $2.2x10^{-16}$. Hence, KED_smn has significantly more trust in the radar information. This could be due to the fact that climatological stations are often located in complex terrain where radar is more uncertain. As KED_all includes these stations in model estimation, we expect the radar-gauge relation to suffer from the larger errors and the βs to be smaller.

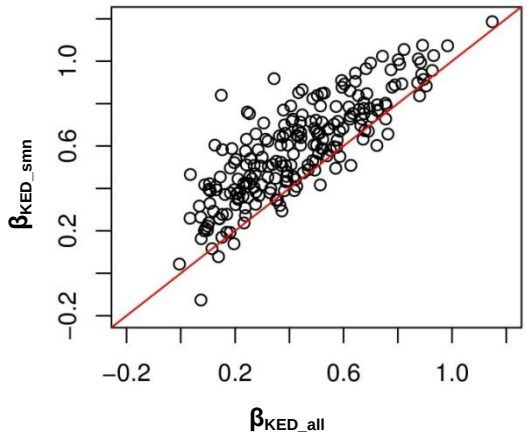

Figure 9 Scatterplot of the estimated radar coefficients β for the two methods KED_all (x-axis) and KED_smn (y-axis). Each dot represents one of the 218 days included in the systematic analysis for the year 2008. The red line shows the location where the βs of both station densities are equal.

4.2.3 Accuracy of point estimates

To assess the accuracy of the point estimates from cross and test data validation, we compare the skill measures of KED to the skill measures of the single-sensor references (OKGAU and RADAR) for the sparse and the dense gauge network. In Table 3, the skill measures are shown for the entire year 2008.

The ranking of the different settings is surprisingly constant among all measures. KED_all always shows most skill, followed by OKGAU_all, KED_smn and OKGAU_smn. Estimating precipitation with RADAR has least skill.

This is most evident considering the Bias. The systematic error of the RADAR is much higher than the error of the geostatistical interpolation method with least skill (OKGAU_smn). Differences between KED and OKGAU with the same number of stations are marginal. They both have a small Bias when the sparse network is used. Adding the climatological gauges renders the estimation

virtually bias-free. An interpretation for this might be the higher relative abundance of climatological gauges located in complex terrain. Neighboring climatological gauges possibly detect precipitation invisible for the radar and missed by the SMN network. Information about this precipitation remains in the model, also if one of the gauges observing it is excluded from model estimation by cross validation. As we will see later on in this section, the Bias can be distorted by compensating positive and negative deviations. We should therefore interpret these results with care.

The Rel. MRTE, a measure of overall quality of estimation, is reduced to a third from RADAR to KED_all. The improvement of KED compared to OKGAU, i.e. the benefit of adding radar information, is more than twice as high when using only SMN stations for model estimation. This does not come as a surprise. We suggest that the additional information provided by the radar is more urgently needed in a low density station network.

Table 3: Skill measures Bias, Rel. MRTE, HK, SCATTER and SEEPS from systematic cross and test data validation for KED and the single-sensor references (OKGAU and RADAR) with the sparse and the dense gauge network. Skill measures are calculated from the pooled results of the 218 wet days of the year 2008.

	Bias (dB)	Rel. MRTE	HK	SCATTER (dB)	SEEPS
RADAR	-0.43	0.37	0.60	2.89	0.41
OKGAU_smn	-0.21	0.21	0.68	1.94	0.31
OKGAU_all	0.06	0.14	0.76	1.49	0.23
KED_smn	-0.20	0.17	0.72	1.74	0.27
KED_all	0.02	0.13	0.78	1.37	0.21

Also for HK, SCATTER and SEEPS, the benefit of adding radar information is higher for the SMN network. Adding information from the climatological gauges, yet, improves the skill measures more strongly than adding radar information. The HK shows a relatively good ability of RADAR to distinguish wet and dry areas. This ability is confirmed by the SEEPS, a categorical measure like HK, showing smaller relative differences between RADAR, KED and OKGAU than the Bias or the Rel. MRTE.

If the skill measures are calculated for the four seasons individually (Figure 10), interesting details become apparent. Yet, the ranking of the different methods for all the measures and seasons stays the same. Whilst the geostatistical methods show a fairly stable Bias for all the seasons, the systematic errors of RADAR differ a lot. RADAR strongly underestimates precipitation in autumn. In summer, the Bias of RADAR relative to OKGAU_smn and KED_smn is small. Here, the compensating effects in the yearly Bias become apparent.

The Rel. MRTE is lowest in autumn and highest in winter for KED and the single-sensor references. KED_smn is particularly skillful and over-performing OKGAU_all in summer. The added value of radar is, hence, particularly pronounced in summer and does exceed that from a dense network.

The strongest variation in the HK for the different seasons is found for RADAR. With RADAR, the distinction between wet and dry areas is best in autumn, i.e. the season where it has the highest systematic errors. The geostatistical kriging methods perform similar in all seasons. Again, KED_smn is equally skillful as OKGAU_all in summer.

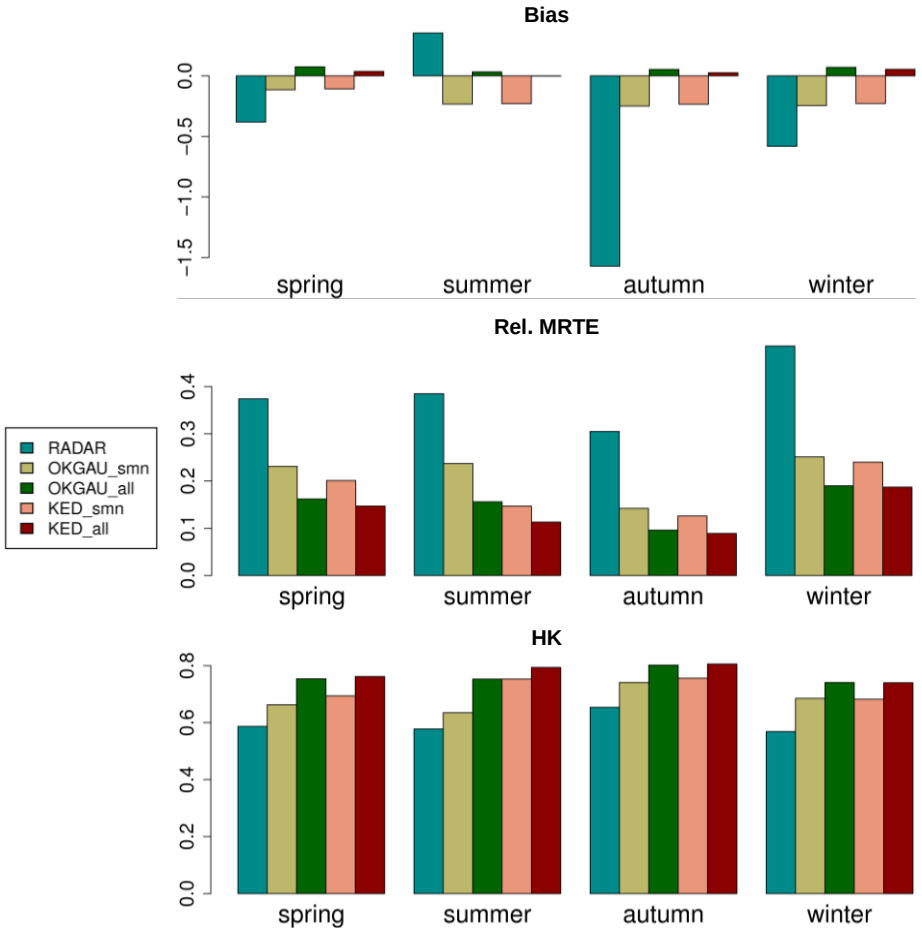

Figure 10 Skill measures Bias (in dB), Rel. MRTE and HK from systematic cross and test data validation for KED and the single-sensor references (OKGAU and RADAR) with the sparse and the dense gauge network. The 218 estimated days are split into the four seasons.

This seasonal analysis suggests that radar information is particularly beneficial in summer. We observe that the relative differences between RADAR and OKGAU_smn, and KED_smn and OKGAU_all are particularly low in summer. In our view, this must be related to the higher abundance of convective precipitation. We understand the strength of radar in convective situations as follows. First, radar provides beneficial information on the fine-scale structure of local convective precipitation cells due to its high spatial resolution. The dense network alone cannot compensate the lack of fine-scale information, because its spacing is still coarse in relation to the typical scale of patterns in summer. Second, convective precipitation is formed in higher altitudes in summer and therefore has better radar visibility. In the three other seasons, however, the added value of the climatological gauges outperforms the additional radar information. The skill of KED_smn is lower than the skill of OKGAU_all. A reason for this is the rather small-scale structure of radar errors (from shadowing by mountains) that is difficult to represent in the trend component of KED. The effective resolution of the precipitation patterns with the dense station network is therefore higher than with the radar.

Figure 11 shows the skill measures for four different regions of Switzerland, namely the Swiss Plateau, the Jura, the Alps and the South. The Bias shows the most complex regional fluctuations of all the analyzed skill measures. These regional fluctuations are stronger for RADAR than for KED and OKGAU. Focusing on the geostatistical interpolation methods, we see that the regional differences with the sparse station network are bigger than with the dense network. The Bias is generally lower when the dense station network is used. Yet, OKGAU_smn and KED_smn have a lower Bias in the Swiss Plateau compared to OKGAU_all and KED_all. Except for the Jura, KED tends to have a lower Bias than OKGAU.

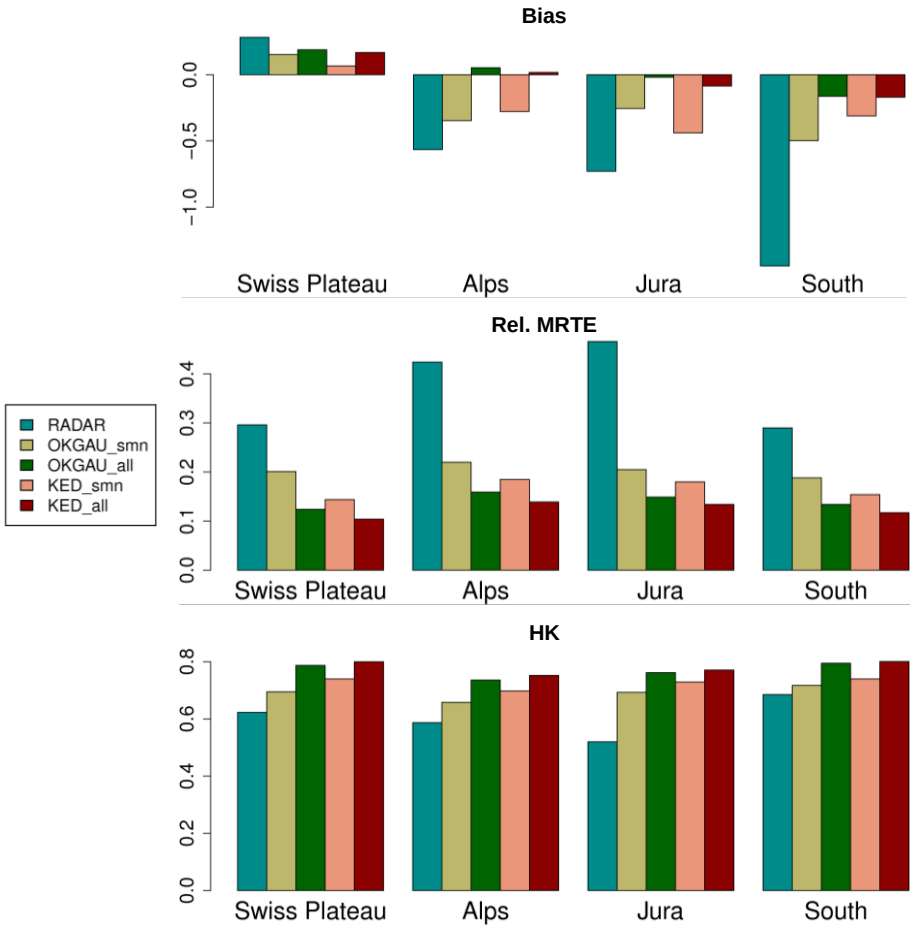

Figure 11 Skill measures Bias (in dB), Rel. MRTE and HK from systematic cross and test data validation for KED and the single-sensor references (OKGAU and RADAR) with the sparse and the dense gauge network. Measures are calculated on the 218 estimated days of 2008 for the four regions Swiss Plateau, Jura, Alps and South individually.

The differences between the regions are surprising. Whilst KED and the single-sensor references all have negative Biases in the Jura and the South, the opposite happens in the Swiss Plateau. The Alps are the only region where the Bias of the different methods reflect the pattern seen in the Bias for all Switzerland. The particularly low alpine Bias of KED_all and OKGAU_all support the aforementioned hypothesis of the beneficial higher abundance of climatological gauges in complex terrain. The regions with positive and negative Bias partly compensate such that the overall Bias is

reduced. More specifically, the positive Bias in the Swiss Plateau is to some degree compensated by the negative Biases in the South and the Jura. The highest absolute compensation is thereby realized for RADAR.

The Rel. MRTE of the geostatistical interpolation methods is, compared to RADAR, low in all regions. Using gauge observations strongly reduce the Rel. MRTE. The combination achieves a further reduction of the estimation errors. The Rel. MRTE is particularly high in the Alps and the Jura. We suggest this to be caused by the reduced radar visibility and a certain underrepresentation of rain gauges in these high-elevation areas.

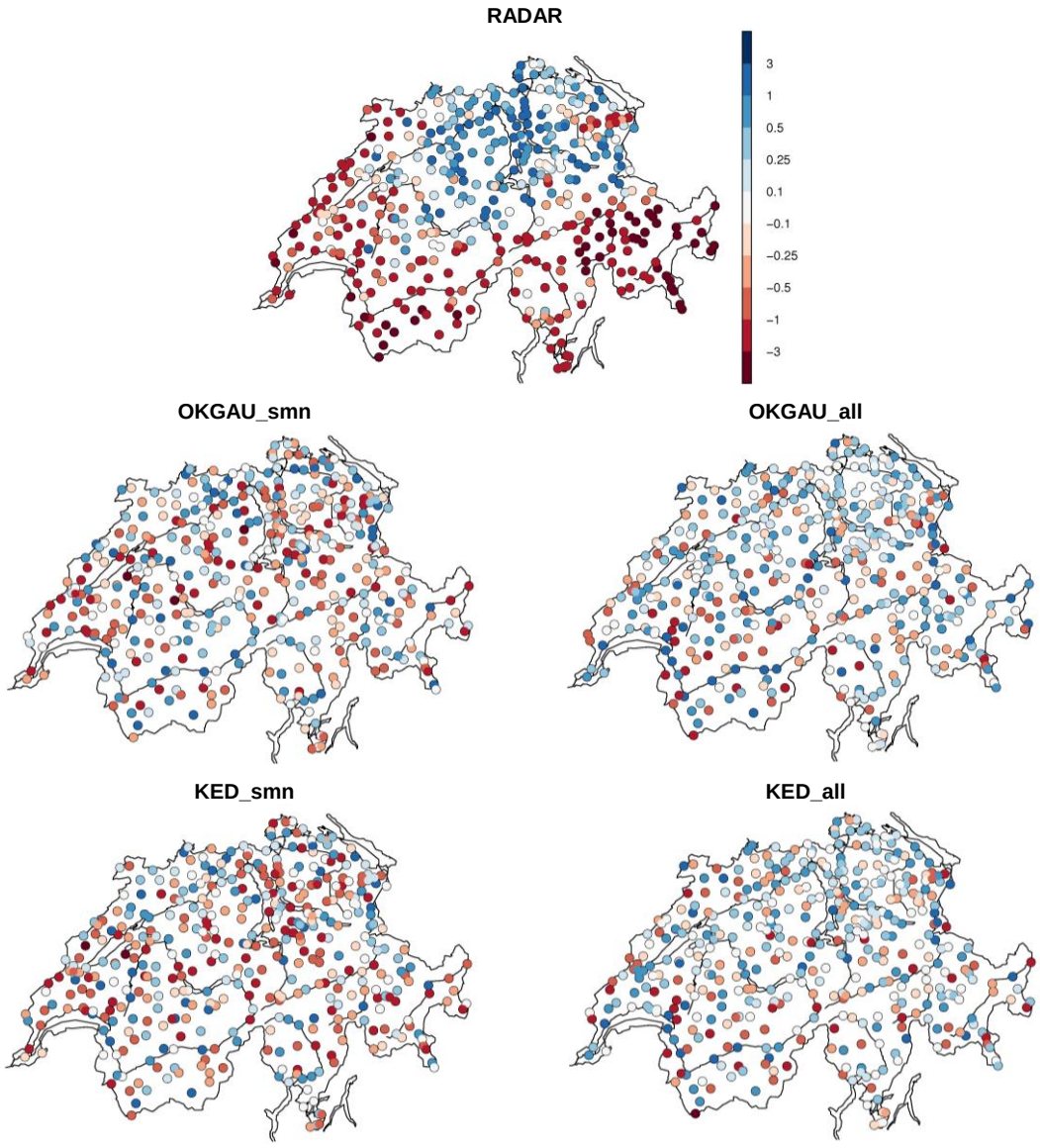

Figure 12 Values of the skill measure Bias (in dB) at all stations individually for KED and the single-sensor references (OKGAU and RADAR) with the sparse and the dense gauge network. Results are shown for the 218 estimated days of the year 2008.

The HK is fairly similar in all regions, i.e. the distinction between wet and dry areas is not so much influenced by regional characteristics. In the Jura the HK of RADAR is particularly low. We interpret this as being caused by radar visibility issues, too. The systematic underestimation of precipitation (i.e. the negative Bias) and the high Rel. MRTE of RADAR in the Jura support this hypothesis. In the HK this can result to some extent in days with wet observations being misclassified as dry days. The inclusion of gauge information increases the HK in all regions. Although OKGAU does not include information on the fine-scale precipitation pattern from radar, the distinction between wet and dry areas has more skill compared to RADAR. The addition of radar information in the combination leads to higher values of the HK in all regions. Still, OKGAU_all outperforms KED_smn and has a HK only slightly smaller than KED_all.

To further highlight how different effects compensate each other in the calculation of the Bias, we zoom into the regions and look at the distribution of the Bias at all station locations. The most remarkable pattern of the Bias (Figure 12) is found for RADAR. There is a strong geographical pattern in the sign of the bias: cross-validated estimations at stations in the South, the Alps and the Jura underestimate precipitation. This underestimation is particularly strong in the Grisons and the Valais. We argue that this underestimation is caused by radar visibility problems in mountainous regions. Contrarily, precipitation is overestimated in northern Switzerland around the Albis radar. There are, however, a few stations in the eastern and western Swiss Plateau region where precipitation is underestimated; most likely, again, due to shadowing by mountains. These stations with negative Bias compensate the overall positive Bias in the region of the Swiss Plateau. The comparatively low positive Bias in the Swiss Plateau (see Figure 11) is, hence, a result of compensatory effects.

None of the geostatistical interpolation methods show this clear a pattern. Positive and negative Biases are distributed more evenly across Switzerland. As the strong north-south gradient of the Bias is not visible with KED, we suggest that the radar-gauge combination is suitable to mitigate the systematic Bias of the radar information. The differences between KED and OKGAU are generally small. Table 3 showed a negative Bias when the sparse and a weak positive Bias when the dense station network is used. This is reflected in Figure 12. With KED_smn and OKGAU_smn, positive Biases seem to be more abundant. Yet, as the negative Biases are stronger in magnitude, they compensate the more numerous but smaller positive Biases. With the dense station network, the Biases seem systematically lower. Compared to KED_smn and OKGAU_smn, the magnitude of the Bias in mountainous regions (especially in the Jura) is lower. Again, we argue this to be related to the higher relative abundance of climatological gauges in complex terrain.

In our view, these plots highlight the partial compensation of positive and negative Biases at individual stations in the overall Bias. The effective compensation might be even larger, since the yearly Bias at one station to some degree includes compensating positive and negative Biases of seasonal precipitation, too.

4.2.4 Reliability of the probabilistic estimate

In this section, we turn away from the point estimates and move towards the probabilistic estimates. As Figure 6 of the previous section, Figure 13 shows the relative frequencies with which measured precipitation falls into the predefined interquantile bins of the pertinent cross-validated probabilistic

estimates. The analysis of the probabilistic estimates is only possible for the geostatistical interpolation methods, as the quantiles are calculated based on the inherent kriging variance. The assessment of the reliability of the probabilistic estimates validates whether this kriging variance describes the uncertainties appropriately. This provides information on how well the simulated observation ensembles discussed in chapter 6 represent the degree of uncertainty inherent in the model.

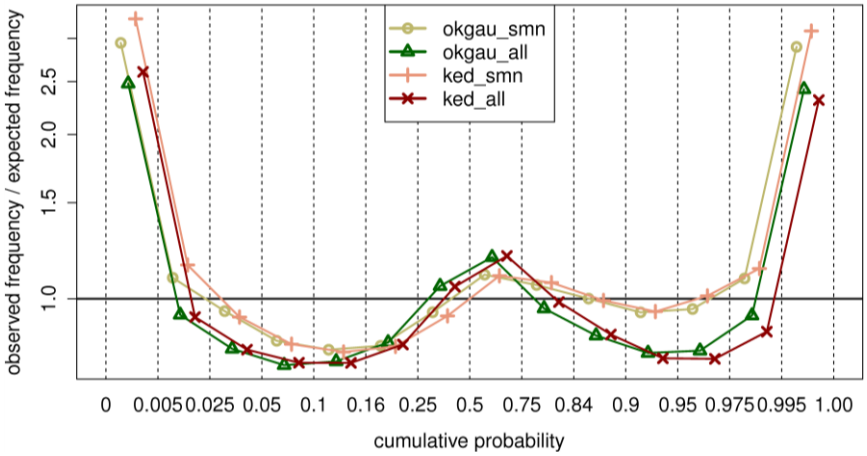

Figure 13 Frequency of gauge measurements to fall in interquantile bins of the pertinent cross-validated probabilistic estimate (x-axis). Frequencies are expressed relative to the expected frequency in a perfectly reliable system on log scale (y-axis). The bins of the distribution are defined by the 0.5%, 2.5%, 5%, 10%, 16%, 25%, 50%, 75%, 84%, 90%, 95%, 97.5%, 99.5% quantiles (dashed vertical lines). Shown are the results from the systematic application over the year 2008 (218 days) for the comparison of the methods OKGAU_smn, OKGAU_all, KED_smn and KED_all.

Both KED and OKGAU produce W-shaped curves. Measurements fall too often below the 0.5% and above the 99.5% quantile. This means that the probabilistic estimates underestimate the true uncertainty in general. The overconfidence in the 0.5% quantile is mainly due to dry stations falling beyond the narrow pdfs when precipitation is weak. This does not raise serious concerns. The apparently strong overconfidence above the 99.5% quantile is caused by only a small part of the observations. Compared to the application of KED with untransformed precipitation data, the reliability is strongly improved (Erdin et al., 2012). Furthermore, measurements fall slightly too often in mid quantile bins and too seldom into moderate lower and upper quantile bins.

The reliability of the probabilistic estimates does not crucially depend on the station density. Still, the geostatistical methods using the same station density are more similar than the ones using the same interpolation technique. Except for the lowest and highest quantiles, the methods using the SMN stations only perform slightly better, i.e. have relative frequencies closer to 1.

The seasonal probabilistic estimates for summer and winter are shown in Figure 14. Looking at the seasons individually confirms the findings drawn for the whole year. There are no extreme deviations apparent. In summer, however, relative frequencies do not go beyond three, whereas they get close to four in winter. For the quantiles above the median, the station density influences the reliability in all seasons.

The differences in the probabilistic estimates among the four dedicated regions are much bigger than the seasonal differences. The reliabilities of the different regions differ in both magnitude and shape. Still, all regions show a kind of W-shape for all the methods. In the South (see Figure 14), the frequency of estimates to fall into the lowest and highest quantile is larger than in the other regions (i.e. stronger overconfidence). This strong overconfidence is seen for OKGAU and KED with both network densities. In the Jura region, the overconfidence is reduced. The reduction is particularly pronounced if ALL gauge observations are used. Whilst the additional radar information does not increase the reliability of the QPE, the increase in reliability due to the climatological gauges is considerable. Estimations in the Alps show most reliability (not shown).

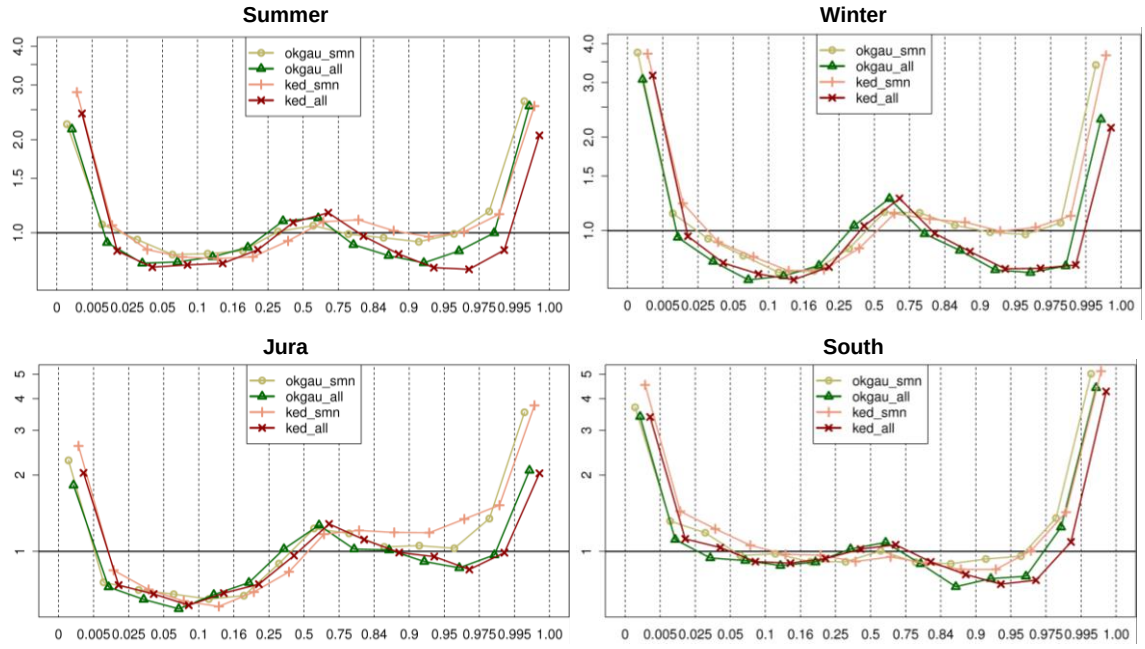

Figure 14 Frequency of gauge measurements to fall in interquantile bins of the pertinent cross-validated probabilistic estimate for the seasons summer and winter (top), and the regions Jura and South (bottom). Legend and axes as in Figure 13. Note that the scale changes from seasonal to regional plots.

Not only the quality of the point estimates but also the reliability of the probabilistic estimates is considerably influenced by regional differences. Can we deduce from this that a stationarity assumption for the whole domain of Switzerland is problematic? The assumption of weak stationarity is certainly a simplification. The reason for the particularly strong overconfidence in the South could lie in the generally more intense precipitation and higher spatial variability compared to the other regions. The estimated variogram for all Switzerland is therefore less representative in the South. As an example, the sill tends to be too small and hence, the pdf of the probabilistic estimate too narrow. Robust regional variogram estimation is, due to the limited data, technically unfeasible and would render the conditional simulation of spatially consistent precipitation fields impossible. Furthermore, a solution at the borders of the regions would have to be found such that the coherence of the estimated precipitation fields is guaranteed.

Table 4: Percentage of measured intense precipitation events exceeding predefined thresholds classified as extremely unlikely (corresponding to the exceeding of the 99.5% quantile) by the pertinent cross-validated probabilistic estimate for OKGAU_smn, OKGAU_all, KED_smn and KED_all. The number of events where measurements exceeded the thresholds and their percentage with respect to all measurements (climatological frequency) are listed.

Threshold	No. of events	Climatological Frequency	Observed frequency in 99.5% quantile			
			OKGAU_smn	OKGAU_all	KED_smn	KED_all
10 mm	17926	11.41%	3.40%	2.46%	3.36%	2.30%
20 mm	7269	4.63%	5.10%	3.70%	4.60%	4.60%
40 mm	1583	1.00%	8.40%	6.50%	6.80%	6.30%
80 mm	138	0.10%	19.60%	13.80%	10.10%	13.80%

Overall, we see that the probabilistic estimates for the entire year over the whole domain smooth out some regional and seasonal deviations. Yet, we do not interpret these seasonal and regional differences as showing major limitations of our method and carry out no further investigations on the issue.

4.2.5 Representation of intense precipitation

Since it is the intense precipitation that causes most damage and harm, its representation is of particular interest in many applications. How well intense precipitation is represented in the QPE is investigated here. We continue the evaluation of the probabilistic estimates specifically for intense precipitation events where measurements exceeded 10, 20, 40 and 80 mm on a single day.

As in Table 2, Table 4 shows the observed frequencies of measured precipitation to be above the 99.5% quantile of its pertinent cross-validated probabilistic estimates. As expected, the fraction of intense precipitation classified as extremely unlikely increases for KED and OKGAU with both station densities for increasing thresholds. As mentioned in section 4.1, restricting the scope to intense precipitation only does not allow the comparison of the observed frequencies above the 99.5% quantile with the expected frequency of 0.5% a fully reliable system would exert when considering precipitation of all intensities. For this reason, we do not know what an appropriate frequency of 'extreme unlikeliness' should be. It is, however, desirable that this frequency stays reasonably small so that a user exploiting the probabilistic estimates can still be confident that the pdfs consider extreme events as possible when they occur.

In general, intense precipitation is well represented by the probabilistic estimate of both KED and OKGAU. As an example, only 14 of the 138 times a rain gauge measured precipitation over 80 mm are considered as extremely unlikely by the probabilistic estimate of KED_smn. The ability of KED_smn to represent intense precipitation is a beneficial prerequisite for the conditional simulation to be performed in the next chapter. There are only marginal differences between KED and OKGAU concerning the representation of intense precipitation. We understand this from the similar reliabilities (Figure 12) of KED and OKGAU. Nevertheless, for the very intense precipitation of over 40 mm, additional radar information seems to reduce the overconfidence.

Figure 15 shows the fraction of observed intense precipitation events exceeding 10 mm classified as extremely unlikely (i.e. the percentage of cases when the measured intense precipitation event falls

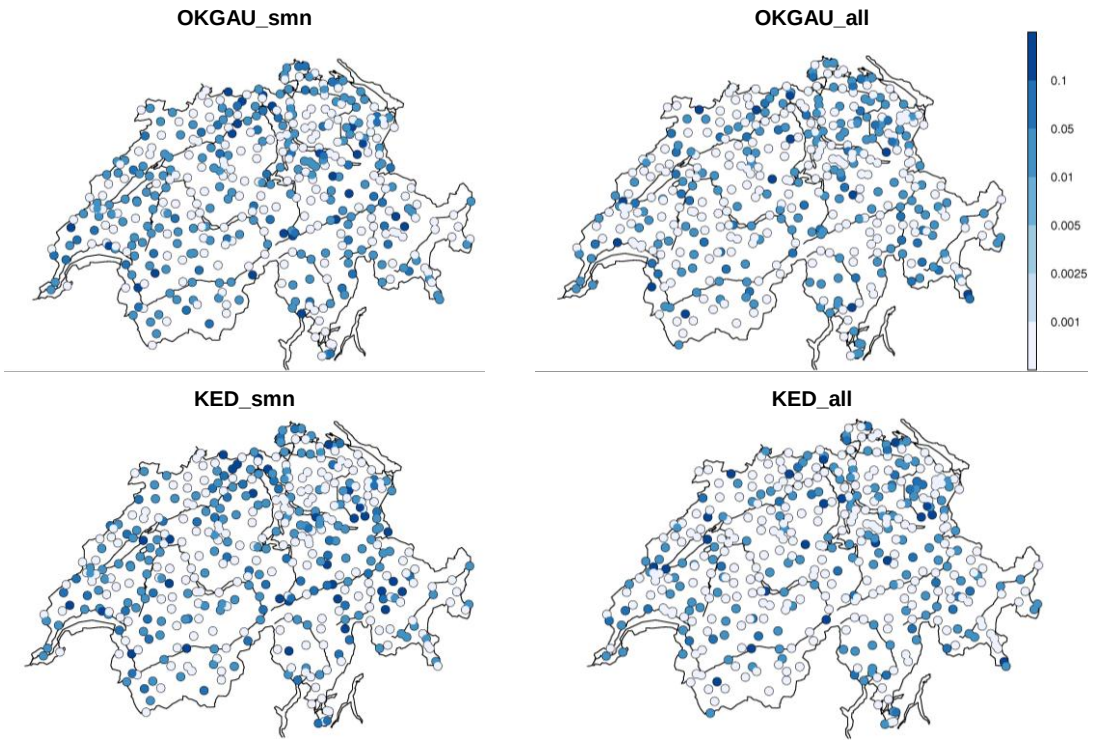

Figure 15 Fraction of measured intense precipitation events over 10 mm considered as extremely unlikely by the probabilistic estimates for OKGAU_smn, OKGAU_all, KED_smn and KED_all. Results are given for each station individually. Extremely unlikely refers to measurements falling into the 99.5% quantile of the pertinent cross-validated probabilistic estimates.

above the 99.5% quantile of its pertinent cross-validated probabilistic estimate, as before) for all stations individually. It can easily be seen that the methods relying on the SMN stations classify precipitation over 10 mm as extremely unlikely more often. We can interpret this, again, with the stronger overconfidence of KED and OKGAU with the sparse station network. Stations with high frequencies of missed intense precipitation are spread all over the domain. The regionally different reliabilities made out in Figure 14 therefore do not manifest when looking at each station separately.

Not only are we interested in the reliability of the probabilistic estimates of intense precipitation, but also in the accuracy of the point estimates. Figure 16 shows the Bias and the MAD for intense precipitation exceeding the thresholds of 10, 20, 40 and 80 mm.

For both skill measures, estimation skills for KED and the single-sensor reference methods RADAR and OKGAU for both station densities decrease as precipitation intensifies. The relative decrease in skill with intensifying precipitation is most extreme for RADAR and OKGAU_smn. How can we interpret this decrease in the quality of the point estimates with intensifying precipitation? We argue that intense precipitation is often particularly localized and cannot be detected extensively by the rain gauges. Any system of spatial analysis is therefore particularly challenged by intense precipitation. Also from the skewness of precipitation data, differences between observed and estimated precipitation tend to be inflated for increased precipitation intensity.

Both the Bias and the MAD can be strongly reduced in the combination. Also concerning the accuracy of the point estimates of intense precipitation, the added value of the climatological gauges is higher than the added value of the radar information. The QPE therefore tend to underestimate intense precipitation in all the considered settings. Again, we understand this as related to the smoothing inherent to any spatial analysis building on 'best estimate' principles, and to the locality of the intense precipitation events. This does not explain the underestimation present in the RADAR estimates, however. One reason for this are the difference in spatial representativity between radar (areal) and gauge (point) observations. These differences are particularly relevant for intense precipitation. The present comparison may therefore be of limited significance.

For the very intense precipitation exceeding 80 mm, the inclusion of radar information in the combination methods is particularly valuable. This strongly increases the skill of the combination with respect to both the MAD and the Bias. Nevertheless, the dense station network leads to a considerable additional improvement also in the combination.

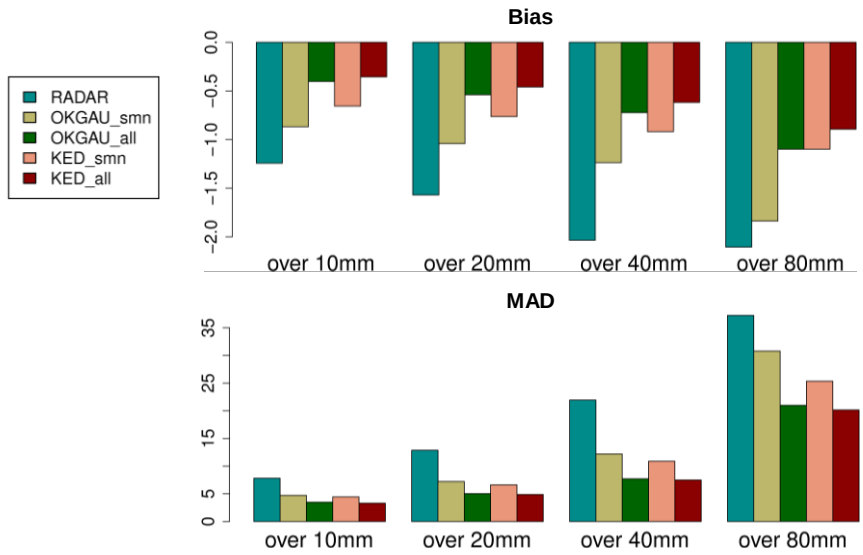

Figure 16 The skill measures Bias and MAD of systematic cross and test data validation with RADAR, OKGAU_smn, OKGAU_all, KED_smn and KED_all. Results for intense precipitation with thresholds of 10, 20, 40 and 80 mm.

4.2.6 Annual precipitation distribution

The aggregated precipitation fields for the entire year 2008 are shown in Figure 17 for RADAR, KED_all, KED_smn and RHIRES. The idea is to compare the annual precipitation distribution of the radar-gauge combinations with RADAR and a deterministic interpolation method exploiting all rain gauge observations and information from topography called RHIRES (we refer to section 3.4.4 for a description of the methodology).

In the yearly aggregation, the challenges to infer precipitation from radar in high-mountain regions and in topographically shielded sections are clearly visible. Especially in the Valais and the Grisons (i.e. the regions where radar information is most erroneous), estimates by RADAR are systematically smaller than by the gauge-based analyses. On the other hand, RADAR seems to overestimate

precipitation in Central Switzerland. There are obvious radar artifacts visible pointing away radially from the Albis radar. These so called radar stripes manifest important visibility problems of the radars that are hard to correct for.

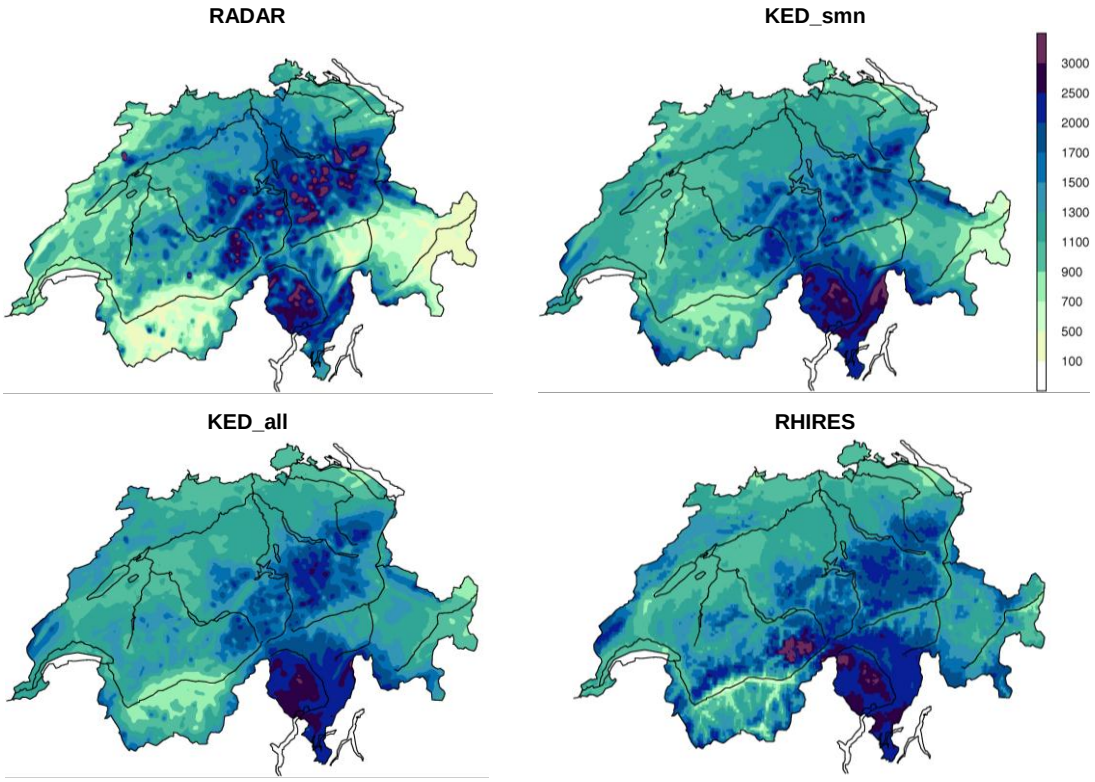

Figure 17 Estimated fields of yearly precipitation in 2008 (in mm) with RADAR, KED_smn, KED_all and RHIRES.

The annual precipitation distribution estimated by KED_smn shows an important improvement over RADAR. Especially in regions where radar estimates are systematically biased, i.e. the Grisons and the Valais, the benefit of the gauge information is evident. The positive precipitation anomaly around the Albis radar in central Switzerland as manifested in the RADAR is not represented here. The radar artifacts are reduced but not entirely removed.

The inclusion of the climatological rain gauges yields further improvements of estimated annual precipitation sums. KED_all produces the smoothest distribution of all methods shown in Figure 17. The radar stripes are hardly visible and estimation in the Grisons and the Valais seem to be more realistic.

The precipitation distribution estimated by RHIRES is the most trustworthy. Especially in the Grisons and the Valais, topographic features are represented more adequately. Yet, the very intense precipitation exceeding 3000 mm in the Jungfrau region has to be considered with care. RHIRES relies on measurements with high uncertainty in this region.

Since the annual precipitation distribution estimated with RHIRES is most trustworthy, we compare it to KED and RADAR. The differences are shown in Figure 18, where red (blue) stands for areas where RADAR and KED estimate lower (higher) precipitation than RHIRES.

The field differences of RADAR show a strong north-south gradient. In Southern Switzerland (including the Jura), RADAR strongly underestimates the annual precipitation sum compared to RHIRES. In the north, it is reverse and annual precipitation is strongly overestimated by RADAR. This north-south difference in radar bias was already highlighted in Figure 12 and is also found in other studies (e.g., Keller, 2012). Furthermore, the radar stripes are clearly visible.

If the SMN stations are added and the precipitation fields are estimated with KED, this north-south gradient is reduced considerably. Positive and negative differences have a more spotty distribution and absolute differences from RHIRES are reduced. Still, there is a tendency to underestimate precipitation in the Valais and the Grisons. Although fairly hidden, the radar stripes are still visible. A strange pattern can be seen in the eastern most part of the Ticino tip, where strong over- and underestimation are next to each other. We expect this to be related to a beam blocking pattern of the Monte Lema radar, possibly enhanced by accidental contrasts in rain gauge measurements between the Southern Grisons and Central Ticino.

Absolute differences and their spatial correlation can be further reduced when the climatological stations are included (KED_all). Although less pronounced, issues pointed out for KED_smn remain problematic in mountainous regions.

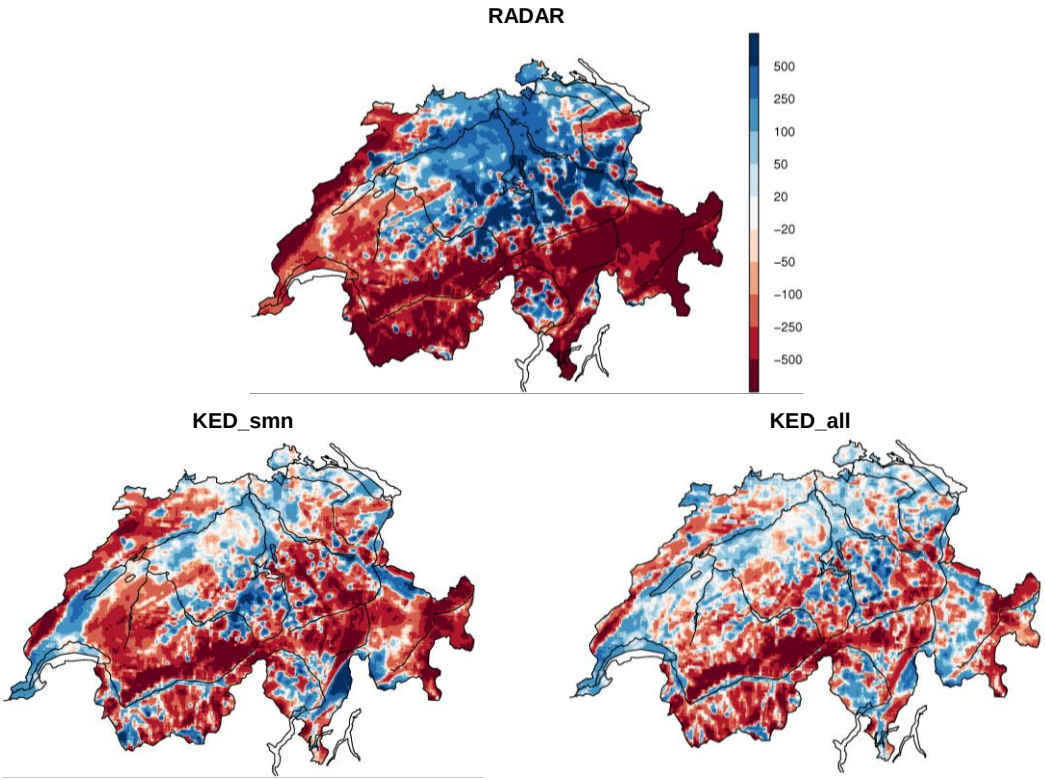

Figure 18 Differences in the estimated fields of yearly precipitation in 2008 (in mm) of RADAR, KED_smn and KED_all compared to the estimated field of RHIRES.

5 Methods ensemble simulation

Conditional simulation refers to the stochastic simulation of random variables with prescribed expected value, spatial covariance structure and the condition that the random variable takes the value of the observation at observation locations. The conditional simulation technique implemented here has the same underlying geostatistical model as KED. The theoretical background thus remains the same and we refer to section 3.1 for the basics of geostatistics. The data for conditional simulation needs to be of Gaussian distribution too. We therefore perform the simulation in the transformed space (see section 3.3 for details on the transformation applied to the data). The precipitation fields are finally obtained by back-transformation.

The chapter is structured as follows. In a first section, the fundamental concept of conditional simulation is illustrated with basic simulation examples. Then we explain how conditional simulation is implemented in this study. A third section discusses how the technical verification of generated observation ensembles is performed and how the degree of uncertainty reduction attributable to different model specifications is computed.

5.1 Fundamentals of conditional simulation

We perform the conditional simulation on the same grid as KED with precipitation simulated on 370x240 grid points. The covariance matrix used to simulate from is so high dimensional that it is difficult to explain the fundamental principle of conditional simulation based on it. We therefore make use of two simple examples here. A more thorough theoretical background can be found in Lantuéjoul (2002), Wilks (2006) and Webster and Oliver (2007).

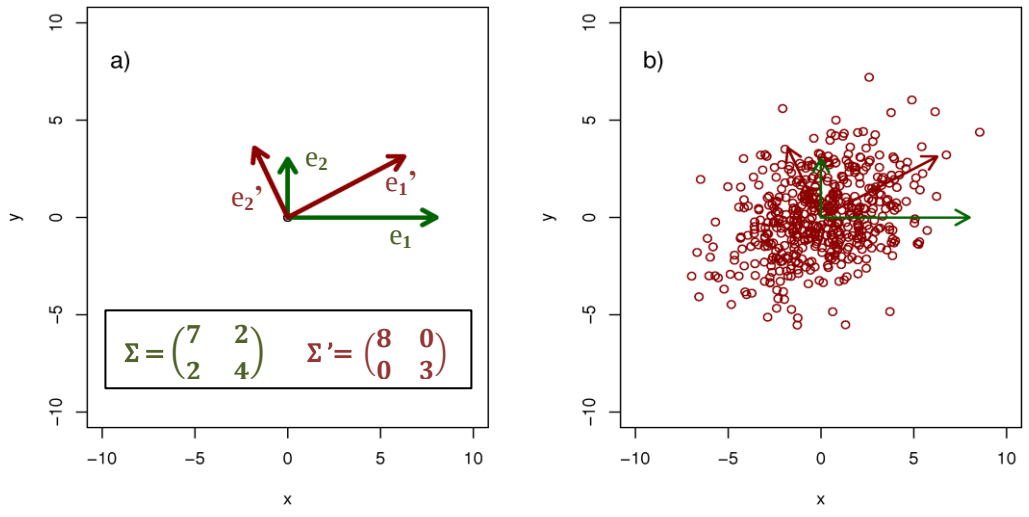

Figure 19 Example simulation of Gaussian distributed two-dimensional random vectors with a predefined correlation and a mean value of $(0\ 0)^T$. a) Eigenvectors of the covariance matrix in correlated (green) and uncorrelated (red) space. The covariance matrices correspond to the respective eigenvectors. The dots in b) represent the Gaussian distributed two-dimensional random vectors x'. A sample of 500 random vectors was simulated. The example is shown in the transformed space (i.e. the eigenspace; the coordinate axes correspond to the alternative orthonormal coordinate system represented by the eigenvectors (Wilks, 2006)).

First, we draw two-dimensional random vectors with normally distributed components that have a predefined correlation (i.e. they are mutually dependent). The conditions of this simulation are fully specified by a vector (2D) of mean values and a covariance matrix (2x2). We refer to Figure 19 for an illustration with a numerical example. The diagonal elements of such a covariance matrix Σ are the variances of the random vector components (S_1 and S_2). As a measure of joint dispersion, the off-diagonal elements are the covariance between the values in both dimensions ($C_{1,2}$).

$$\Sigma = \begin{pmatrix} S_1 & C_{1,2} \\ C_{1,2} & S_2 \end{pmatrix} \quad (2)$$

Unless these off-diagonal elements are zero, the values are correlated.

It is most convenient to perform the simulation in a transformed coordinate system, where the two (transformed) vector components are uncorrelated. This permits the application of conventional univariate random number generators, sequentially for the two vector components. Transformation of Σ into uncorrelated space can be achieved through eigenvalue decomposition.

$$\Sigma \cdot e_k = \lambda \cdot e_k \quad (3)$$

where e_k are the eigenvectors (e_1 and e_2) and λ the eigenvalues (i.e. the variances along the eigenvectors). The eigenvectors have unit length, are orthogonal to each other and can be interpreted as an alternative orthonormal coordinate system (Wilks, 2006). The matrix E with the e_k in the columns

$$\mathrm{E} = [e_1\ e_2] \quad (4)$$

can be used to diagonalize Σ.

$$\Sigma' = \mathrm{E}^T \cdot \Sigma \cdot \mathrm{E} \quad (5)$$

yields the diagonalized (i.e. uncorrelated) covariance matrix Σ'. Σ' has the eigenvalues as diagonal elements and zeros in the off-diagonals. With the aid of a random number generator, a set of n random numbers is drawn based on the prescribed variances in the diagonal elements of Σ'.

Finally, the simulated random vectors x' in uncorrelated space are back-transformed into correlated space using the following relation:

$$\mathrm{x} = \mathrm{E}^T \cdot \mathrm{x}' \quad (6)$$

where x is the desired matrix of correlated two-dimensional random vectors.

In a second example, we show how random numbers along a transect are simulated from a prescribed variogram. Figure 20 provides numerical examples. As a first step, we specify the variogram γ (Figure 20 a) and c)). We use an exponential variogram model with the parameters *partial sill* (σ^2_{ps}), *nugget* (σ^2_n) and a *range* parameter r corresponding to a third of the practical range.

$$\gamma(\mathrm{h}) = \sigma_n^2 + \sigma_{ps}^2 \cdot (1 - exp[-\frac{\mathrm{h}}{\mathrm{r}}]) \quad (7)$$

With this variogram, we can compute the semivariance between two arbitrary points depending on the lag distance h between them.

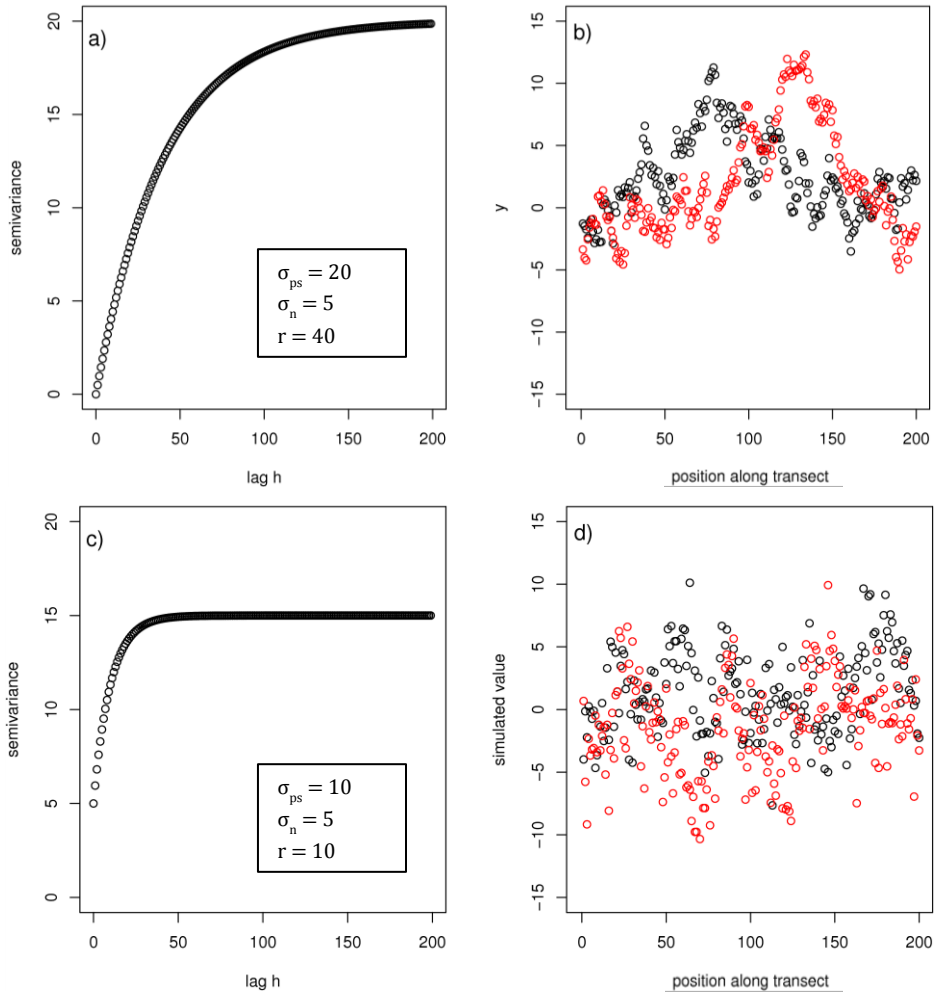

Figure 20 Example simulations of correlated random numbers with prescribed variogram. a) and c) are two examples of an exponential variogram with specified variogram parameters partial sill (σ^2_{ps}), nugget (σ^2_n) and a range parameter (r; corresponding to 1/3 of the practical range). b) and d) both show two realizations (black and red) of a random vector with 200 components simulated with an expected value of 0 and the example variogram from a) (for b)) and c) (for d)).

To generate the correlated random numbers, we use a covariance function. Assuming weak stationarity, the covariance function C is directly linked to the variogram according to the following relation.

$$C(h) = C(0) - \gamma(h) \qquad (8)$$

The covariance is again a function of the lag h and C(0) is the total variance of the random variable (i.e. $\sigma^2_n + \sigma^2_{ps}$). The covariance function C(h) is therefore

$$C(h) = \begin{cases} \sigma_{ps}^2 \cdot \left(\exp\left[-\frac{h}{r}\right]\right) & for\ h > 0 \\ \sigma_n^2 + \sigma_{ps}^2 & for\ h = 0 \end{cases} \quad (9)$$

Equation (9) is used to build the symmetric covariance matrix Σ with nxn dimensions. The covariance between every pair is written into Σ as illustrated in Figure 21.

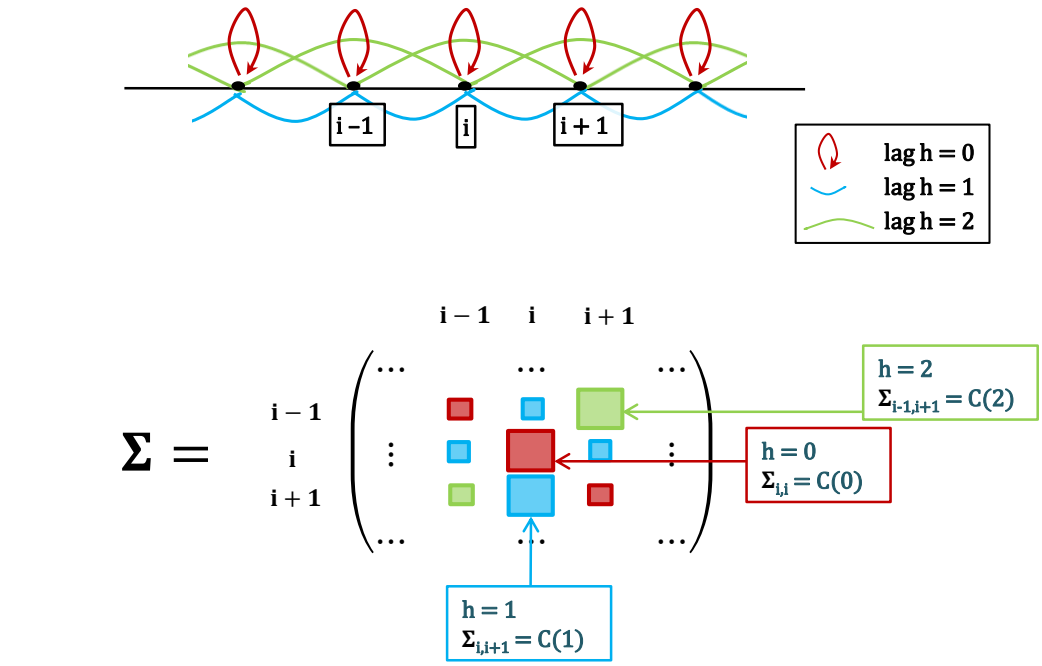

Figure 21 Example of how the nxn dimensional covariance matrix Σ is built for unconditional simulations.

Once the covariance matrix is built, we can proceed analogously to the first example. We diagonalize Σ according to equation (5), simulate the components of the random vector and back-transform them with equation (6). Figure 20 b) and d) show example realizations of such an unconditional simulation.

To promote an intuitive understanding of conditional simulation, we made use of simple examples of unconditional simulation. Turning towards the conditional simulation of precipitation studied in this thesis, the level of complexity increases in two ways. On the one hand, we perform the simulation on the two dimensional target grid covering the territory of Switzerland. On the other hand, we no longer perform unconditional simulations but condition the random variable on the gauge observations at gauge locations. The simulated random numbers at gauge locations adopt the observed values there. The conditioning is performed as follows. Random numbers are simulated unconditionally first. The actual conditioning is achieved through the subsequent correction of the unconditional random field. Lantouéjoul (2002) propose the following algorithm for the correction of a Gaussian random field with the conditioning data (i.e. the available observations). The simulated unconditional random numbers are picked up at each observation location and subtracted from the observation to yield the difference between the simulated unconditional value and the observation. The random number from unconditional simulation for each grid point is then corrected with a weighted linear combination (with weights determined by the range of the underlying variogram) of the aforementioned differences at

observation locations. It can easily be verified that such an algorithm honors the conditioning data and does not alter the unconditional simulation where grid points are out of the range of the conditioning data (Lantouéjoul, 2002).

How we implement conditional simulation under these circumstances is explained in the next section.

5.2 Implemented method for conditional simulation from combined radar-gauge precipitation data

As pointed out in the introduction to this method section, the implemented procedure to generate observation ensembles with merged radar-gauge data is based on the same geostatistical model as KED (see section 3.2). A random conditional realization is described as a multivariate Gaussian distributed random vector with an expected value defined by the trend of the KED and a covariance matrix defined by the semivariance function of the KED residuals. We adapt equation (1) from KED for the purpose of conditional simulation. The deterministic part (i.e. the trend or drift) remains the same. The difference between KED and conditional simulation manifests in the stochastic part.

In this stochastic part, we simulate a field of residuals. This simulated residual field represents the positive or negative deviations from the deterministic part. Two conditions are imposed on the simulation. First, the residual field is simulated based on the variogram previously estimated within KED. A detailed description of the variogram fit is provided in section 3.3. Second, the simulated residual field at rain gauge locations is conditioned on the observed deviation of the gauge observations from the trend at rain gauge locations.

Once the residual field is simulated, we add the deterministic trend field to it. The result of this combination is the precipitation field in transformed space. If we simulate n fields of residuals, add the trend field to all of them and apply the inverse Box-Cox transformation (i.e. back-transform into precipitation space), we get an ensemble of n precipitation fields. Each ensemble member represents a realization of the unknown true precipitation field. The resulting fields are interpreted as arrays of point values rather than grid pixel averages. They refer to a possible precipitation amount a gauge situated at the center of the pixel would measure. Figure 22 provides a summary of the procedure.

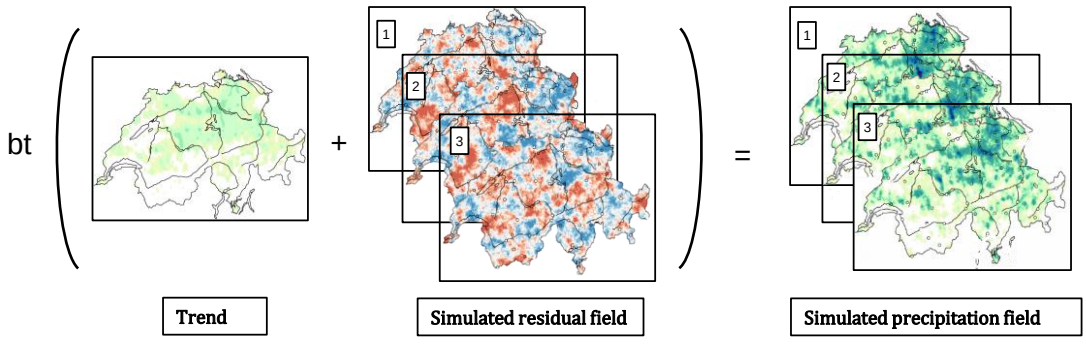

Figure 22 Overview of the implemented procedure for the conditional simulation of precipitation fields. One realization of the residual field is added to the deterministic trend to yield a realization of the precipitation field in transformed space. Subsequent back-transformation (bt) results in the simulated precipitation field in the precipitation space. The number in the box refers to the specific ensemble member.

5.3 Discussion of characteristics of the generated observation ensembles

As the true precipitation field is unknown, we cannot truly evaluate the plausibility of the observation ensembles generated. In some studies (e.g. Clark and Slater, 2006), cross validation was used to analyze the estimation quality of conditional simulation. We already evaluated the reliability of the cross-validated probabilistic estimates from KED in section 4. Here, we check whether the ensembles reproduce the prescribed spatial characteristics. We can also modify specific model settings and investigate their influence on the uncertainty in the observation ensembles.

5.3.1 Technical verification of generated observation ensembles

We verify the technical implementation of the conditional simulation procedure in two ways. First, we check whether the estimated fields reproduce the underlying variogram, i.e. the variogram fitted to the original data. We take a random sample of 500 grid points spread all over Switzerland, fit an exponential variogram to the sample with MLE and compare the fitted to the underlying variogram.

Second, we investigate whether the spread of the ensembles approximates the kriging standard spread for increasing numbers of simulations. We use the following robust spread measure (r.sd):

$$\mathrm{r.sd} = \frac{1}{2} \cdot (\mathrm{Q84} - \mathrm{Q16}) \qquad (10)$$

where Q84 and Q16 are the 84% and the 16% quantiles of the ensembles. This choice is motivated by the skewed nature of precipitation data. For an infinitely big ensemble, the differences between the ensemble and kriging spread should vanish. We compute the differences to kriging with ensembles of 10, 100, 200 and 500 members. These experiments also provide insight about the number of ensemble members needed to appropriately describe the uncertainties.

5.3.2 Comparison of spatial uncertainty

Whether the generated observation ensembles plausibly reproduce spatial uncertainties in precipitation fields is investigated here. We study the influence of the network density, the precipitation situation, the ensemble size, the temporal resolution and the addition of radar information.

The uncertainty experiments are based on the mean areal precipitation of a catchment. For every ensemble member, the areal means of the Reuss and the three nested sub-catchments of decreasing size, Reuss Luzern, Urner Reuss and Schaechenbach (see Figure 23), are calculated. We use the robust spread measure r.sd normalized with the median of the ensembles as measure of relative spatial uncertainty.

We performed the following experiments:

- Conditional simulation from combined radar-gauge data (CSCOMB) with 100 ensemble members and the SMN station network for three different days (8 August 2007 (stratiform precipitation), 10 June 2008 (isolated convective precipitation) and 6 September 2008 (overall convective precipitation))

- CSCOMB with the SMN network for 10 June 2008 with 10, 50, 100, 200 and 500 members
- CSCOMB and conditional simulation from gauge data only (CSGAU) with 100 members for all the example days and the station networks ALL and SMN
- CSCOMB with 100 members and the SMN network for monthly sums of daily precipitation in January, May and July 2008

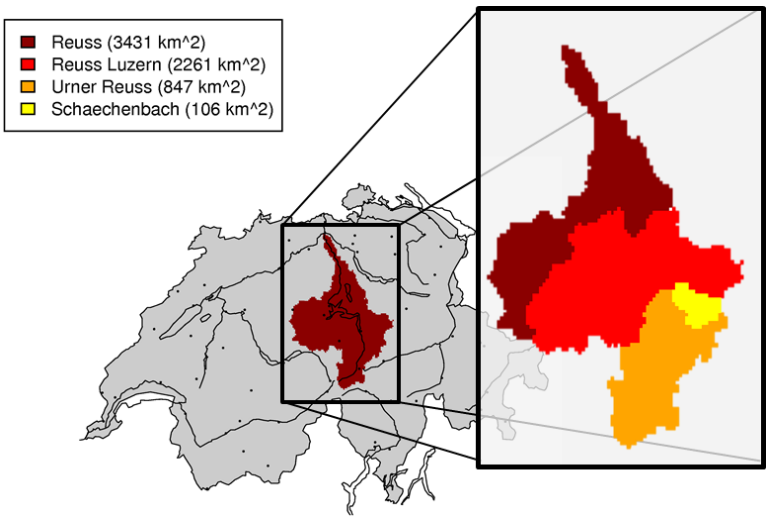

Figure 23 Location of the Reuss catchment in Central Switzerland. The detail shows the borders of the Reuss catchment and the nested sub-catchments.

For ease of understanding, we again introduce a nomenclature for the different conditional simulation settings compared. CSCOMB_all and CSCOMB_smn refer to the conditionally simulated observation ensembles generated with merged radar-gauge data and the station networks ALL and SMN. Ensembles from conditional simulation of gauge observations only are referred to as CSGAU_all and CSGAU_smn respectively.

5.4 Software

The software used is the same as in section 3.5. For the conditional simulation of the residuals, we us an additional R-package called RandomFields (Schlather, 2001).

6 Results from simulated observation ensembles

Results from the conditional simulation experiments are presented here for three example days. The chosen example days represent characteristic precipitation situations encountered in Switzerland and are described in section 2.2. The chapter is structured as follows. Section 1 discusses the technical verification of generated observation ensembles. Exemplary precipitation fields from conditional simulation are shown in section 2. The last section is dedicated to experiments about the influence of different method settings on the spatial uncertainty in the ensembles.

6.1 Technical verification of the ensembles

Results from investigations whether the generated observation ensembles comply with the underlying geostatistical model are presented here. Firstly, we show whether the spatial covariance in the simulated precipitation fields reproduce the underlying variograms, i.e. the variograms that were estimated from the original data. Secondly, we discuss if the ensemble spread at the grid point scale reproduces the uncertainty distribution implied by the underlying stochastic concept (i.e. the spread implied by the kriging standard spread). All the simulations of this technical verification are performed with CSCOMB_smn. CSCOMB_smn serves as an example for illustration.

In order to investigate the reproduction of the spatial covariance structure in the simulated residual fields, we took ten ensemble members of CSCOMB_smn. From each of the ten members, we take five random samples of 500 points. We fit to all of this 50 sets of 500 synthetic stations an exponential variogram. The distribution of the fitted variogram parameters partial sill and nugget are shown in Figure 24 for all the three example days.

For the estimated partial sills, we find a spread of the fitted values on all the example days. On the 10 June 2008, the median of the 50 variograms slightly deviates from the underlying partial sill (represented by the black cross). Overall, we argue the spread and the small deviations of the median from the underlying partial sill to be in line with the random deviations we would expect.

There is a spread of the fitted nuggets on all the example days. However, no systematic deviation of the fitted nuggets from the underlying nugget is indicated. We again suggest the findings to be within the scope of random fluctuations.

The range was reproduced perfectly for all the ensemble members, samples and days (not shown). The implemented conditional simulation procedure therefore seems to have particular strength in reproducing the underlying range over which observations are correlated.

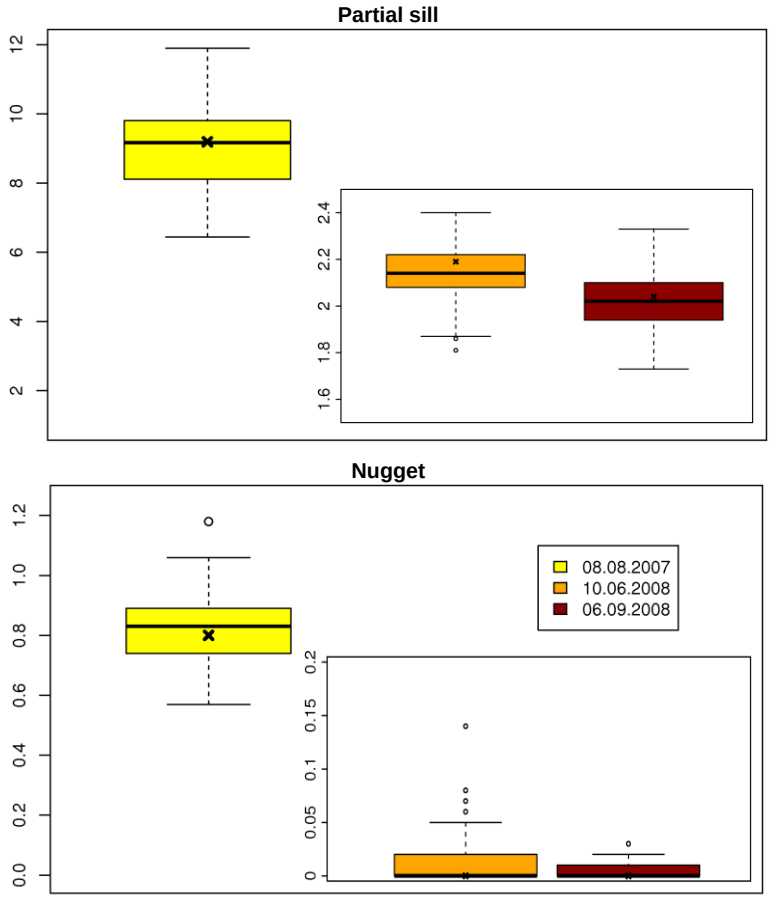

Figure 24 Boxplots of the fitted variogram parameters partial sill and nugget for the three example days. Exponential variograms were fitted with MLE to ten ensemble members from CSCOMB_smn at five random samples of 500 points. The boxplots show the distribution of the fitted variogram parameters from these 50 variograms. The black cross represents the underlying variogram parameter of CSCOMB_smn on the specific day.

How do we interpret the perfect reproduction of the range in contrast to the considerable spread of estimated partial sills and nuggets? We can imagine this to be related to the variogram fitting technique used here, which tends not to reject the supplied initial value from the empirical variogram for the range. Nevertheless, the random deviations observed between the estimated partial sills and nuggets are not contradicting our expectations. The simulated precipitation fields, moreover, are never used individually. For the following investigations and in applications using conditional simulation, we always consider an independent ensemble of simulated precipitation fields. We therefore view the ability of the ensembles to represent the spatial covariance structure of the original data as verified.

We now turn towards the analysis of the standard spread between the simulated precipitation fields in the ensembles. Figure 25 shows the robust standard spread r.sd (see equation (10)) of the ensembles from CSCOMB_smn on the 8 August 2007 for ensemble sizes of 100, 200 and 500 members. The kriging r.sd is shown, too. As expected, the ensemble spread approaches the kriging spread more and more with increasing numbers of simulations. The basic spatial structure of the spread is already captured with 100 simulations. However, there is still a lot of small-scale variance

in the ensemble spread. This small-scale variance is strongly but not entirely removed in the ensemble with 500 members.

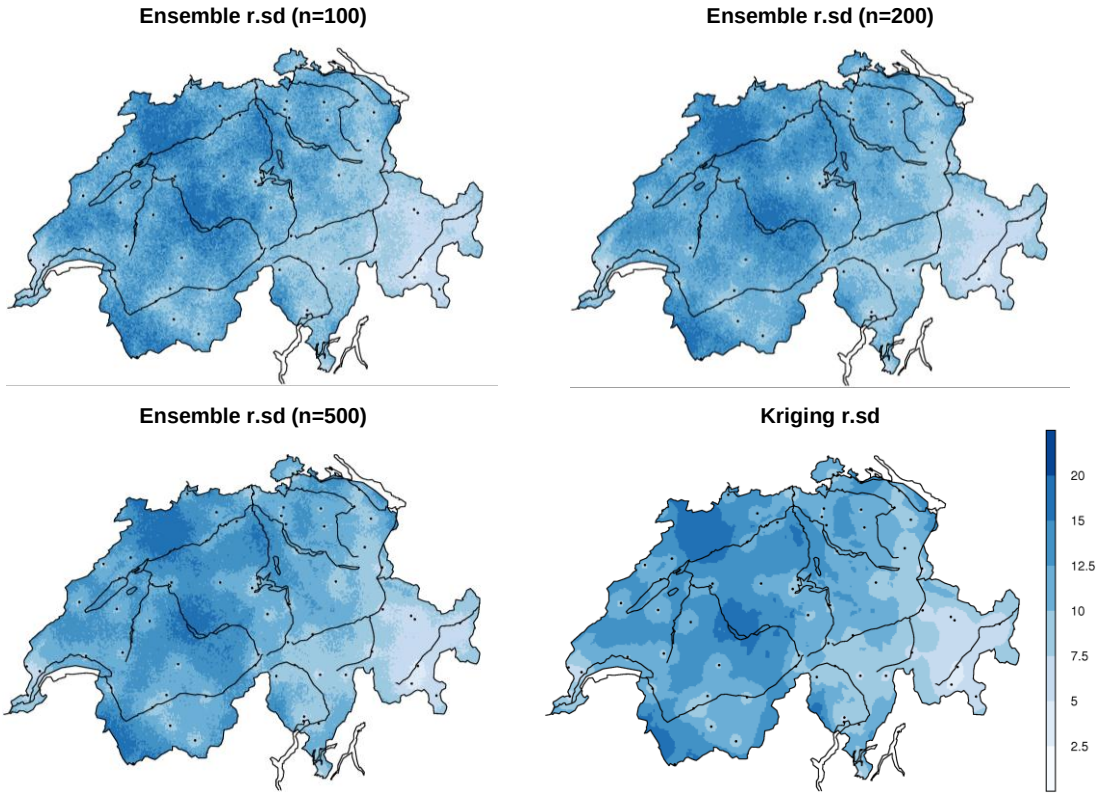

Figure 25 Ensemble r.sd from CSCOMB_smn for ensembles of 100, 200 and 500 members and kriging r.sd from KED_smn on the 8 August 2007 in mm. The robust spread measure r.sd is defined in equation (10). See Figure 2 for an illustration of the precipitation situation on the 8 August 2007.

We understand this approximation as follows. The simulated ensemble can reproduce the theoretical spread (inferred from the kriging standard spread) only with limited accuracy when the size of the ensemble is small. A small ensemble under-samples the joint pdf, which reflects in a noisy variation of r.sd between neighboring grid points. An ensemble with 500 realizations, however, reproduces the pattern and magnitude of the theoretical spread accurately, confirming the technical consistency of the simulation approach with the underlying stochastic model.

Further peculiarities are the distinct minima of the spread around gauge locations represented in all the four plots. We expect to find those minima due to the conditioning of the simulation on the gauge observations. Since the covariance over short distances is high, the scope for random deviations is smaller close to the gauges. The variance between the ensemble members is therefore small. A last point we want to highlight is that we show the absolute spread in physical (i.e. untransformed) space here. The back-transformation leads to large spreads in regions with intense precipitation (see Erdin et al., 2012). We therefore interpret the maxima in spread in the north of Lake of Biel and around the Lake of Thun as products of two different processes. These processes are first, the lack of a rain gauge in near proximity and second, the high amount of precipitation realized there.

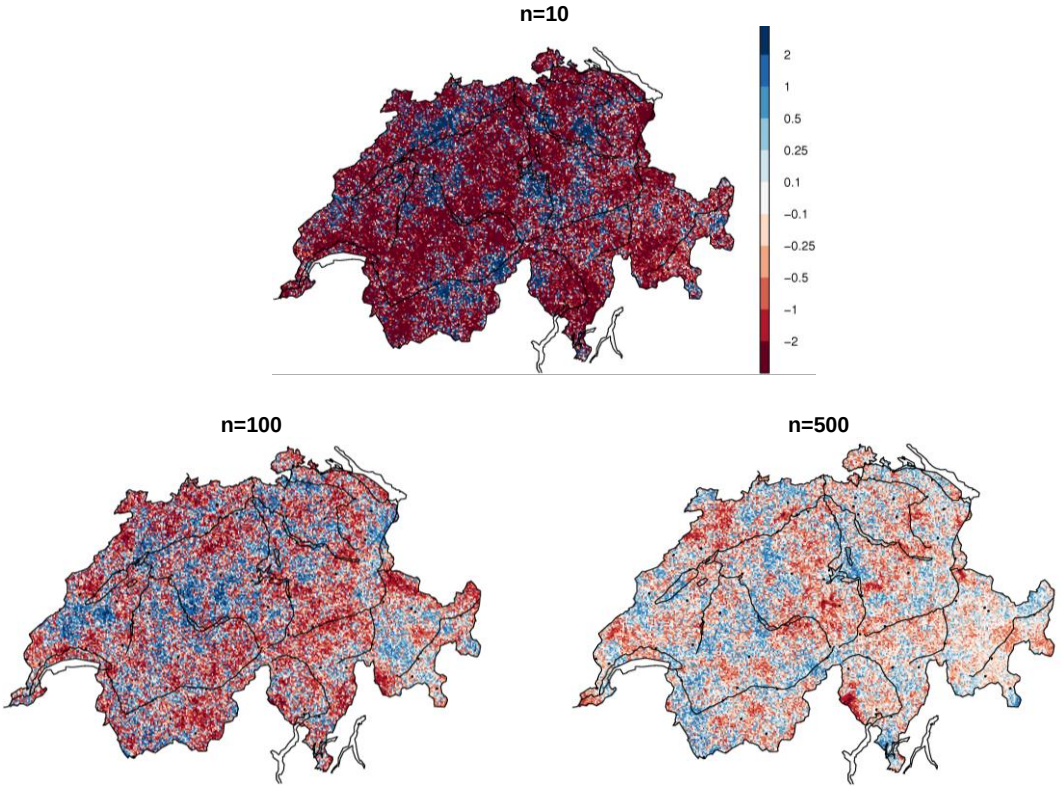

Figure 26 Differences between the ensemble and kriging r.sd for ensembles of 10, 100 and 500 members on the 8 August 2007 in mm.

To highlight the deviations of the ensemble and the kriging standard spread, we show their differences in Figure 26 for ensembles of 10, 100 and 500 members. Positive (blue) values indicate regions where the spread in the ensembles is bigger than the kriging spread. As pointed out before, the differences between ensemble and kriging r.sd are reduced when the ensemble size is increased. The reduction is particularly strong when increasing the number of ensemble members from 10 to 100. In all the plots, the positive and negative deviations are spread all over the domain. They are correlated in close proximity with a lot of small-scale variance. This correlation originates from the spatial correlation. The small-scale variance, too, stems from the nugget in the original data and was already seen in the ensemble r.sd. The nugget effect, i.e. the strong small-scale variance caused by the nugget, will be supported when we look at the other example days afterwards.

The eastern part of the Grisons shows the random nature of positive and negative differences between the ensemble and the kriging spread: the sign changes between the ensemble sizes. The differences are, however, related to maxima and minima of the spread. As the intensity of precipitation and thus, the model spread are quite uniform here, these maxima and minima are not very pronounced. Nevertheless, the reduced difference of ensemble and kriging r.sd in the Grisons (i.e. the region where the model spread is particularly small) is visible.

Up to now, we focused on the 8 August 2007 in this discussion of the spread in the observation ensembles. The two convective days, i.e. the 10 June 2008 and the 6 September 2008, reflect what

we have found for the day of stratiform precipitation. For the sake of completeness, we provide a short discussion and show figures of ensemble and kriging r.sd for both convective days in the appendix section A.

Summing up the above results, we find the spatial covariance structure imposed by the underlying variogram to be well reproduced in the ensembles. The spread of the simulated ensembles with many ensemble members reflects the theoretical model spread well. Our technical implementation of the conditional simulation procedure is hence verified to be successful. We suggest these findings to be transferable to ensembles generated with the single-sensor reference and the dense station network. With a well-justified confidence in the simulated fields we go about to investigate the generated precipitation fields.

6.2 Precipitation fields from conditional simulation

The chosen example days (see Figure 2 and section 2.2) are used to illustrate how precipitation fields from conditional simulation actually look like. Here, we point out the differences between conditional simulation and the best estimates from kriging, and show qualitatively how strong the random deviations between the individual ensemble members are. The 10 June 2008 is selected for in-depth discussion as it highlights many remarkable features of conditional simulation and was already discussed as example case in section 4.2.1. For the remaining two example days, we briefly point out the important peculiarities and refer to the appendix (section B) for the figures and a more detailed description.

Figure 27 shows the precipitation fields from kriging (i.e. the field of best estimates) and conditional simulation for the combination and the single-sensor reference method with both station networks. For comparability, the radar composite with the rain gauge measurements from the dense station network is shown in Figure 2. In the best estimates, areas with the same precipitation amount estimated are larger than in the realizations from conditional simulation. All the ensemble members from CSCOMB and CSGAU for both network densities have a higher spatial variability of precipitation than the corresponding best estimates. The fields of best estimates are therefore much smoother than the simulated precipitation fields. A comparison between the combination and the single-sensor reference accentuates the strong increase in the variability of precipitation from OKGAU to CSGAU. The best estimates of OKGAU with both station densities are very smooth. The ensemble members from CSGAU, however, have a spatial variability representing the spatial covariance structure of the original data. The increase in spatial variability from the best estimates to the simulated fields of the combination (KED to CSCOMB) is less pronounced. The inclusion of radar as an external drift variable leads to considerable spatial variability already in the field of best estimates. Still, the increase in small-scale variability of precipitation in the ensemble members is clearly discernible. The quantitative differences between the precipitation fields OKGAU and CSGAU, however, do not imperatively have to be bigger than the differences between KED and CSCOMB.

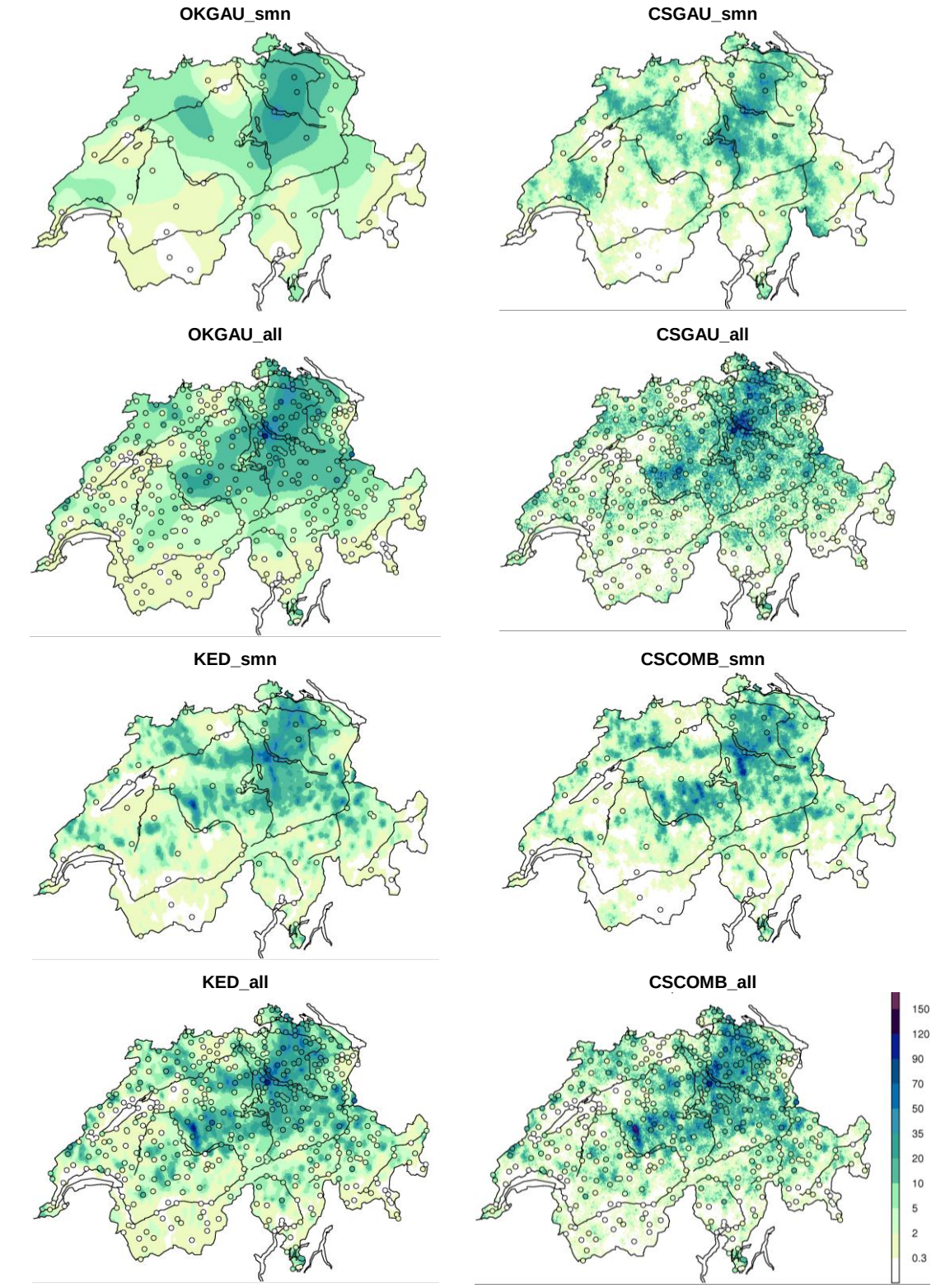

Figure 27 Best estimate fields of precipitation (in mm) from kriging (left) and one ensemble member from conditional simulation (right) on the 10 June 2008. Precipitation fields are shown for the single-sensor reference method (OKGAU and CSGAU) and the combination method (KED and CSCOMB) for both network densities.

Conditional simulation produces local extremes beyond the range of the observations. More frequent are both areas where very intense (e.g. the Lake of Zurich area) and spots where no precipitation at all (e.g. the Valais) is simulated. The additional radar information in CSCOMB seems to increase the likeliness of extreme precipitation over 90 mm. We would expect this behavior, since the trend field from radar includes maxima lying between the stations. These maxima are not reproduced in simulated precipitation fields from CSGAU with a constant underlying trend corresponding to the mean of the rain gauge observations.

Comparing fields using the sparse and the dense station network for model estimation and conditioning, we find the additional climatological gauges to lead to an increase in small-scale variability. We understand this from the differences in the nugget between the dense and the sparse station network. Whilst CSCOMB_smn and CSGAU_smn both have a nugget of zero, the nugget-to-sill ratios are more than 0.3 and 0.2 for CSCOMB_all and CSGAU_all respectively. This renders the simulated precipitation fields spottier. (A nugget of zero is more frequently realized when using the sparse station network due to the implemented variogram modeling procedure).

The example demonstrates the differences between the fields of the best estimates and realizations from conditional simulation. The best estimates indicate for every grid point the values which have on average the least squared deviation from the true (but unknown) precipitation field. This implicitly entails a smoothing of the precipitation field. The best estimates therefore clearly miss small-scale variations present in the original data. If a variogram was estimated from such a field of best estimates, the variance would be much smaller than the variance present in the original data. Precipitation fields from conditional simulation retain this variance. The simulated ensemble members are all equally probable and represent potentially true precipitation fields. In these precipitation fields, extremes are represented exceeding the range of the gauge observations and, in case of the combination, the adjusted radar information.

It is difficult to assess whether the small-scale structure evident in the simulation for the 10 June 2008 from CSCOMB_all is truly realistic for a precipitation field. Indeed, the comparatively large nugget could be a manifestation of the limited spatial representativity of the gauge measurements. In this case the variations from one grid point to the next contain a component of variation that is due to variations at very small scales (including random measurement errors). The construction of our simulation system via point measurements in fact presumes that the resulting fields are interpreted as an array of point values (say the measurements at rain gauges located at the center of the grid pixels), rather than a field of areal averages over the grid pixels.

Four ensemble members from CSCOMB_smn are shown in Figure 28. They obviously look very similar. The underlying spatial covariance structure and the values at gauge locations are by definition the same. What makes the individual ensemble members unique are their random deviations in between rain gauge locations. As shown in Figure A1 of the appendix, these deviations (i.e. the r.sd) are largest where precipitation is most intense. An example of a region where the ensemble members strongly deviate from each other is in between the lakes of Zurich and Zug. Whilst member a) has a strong maximum with precipitation reaching up to 120 mm, ensemble member d) does not show a distinct maximum in this region.

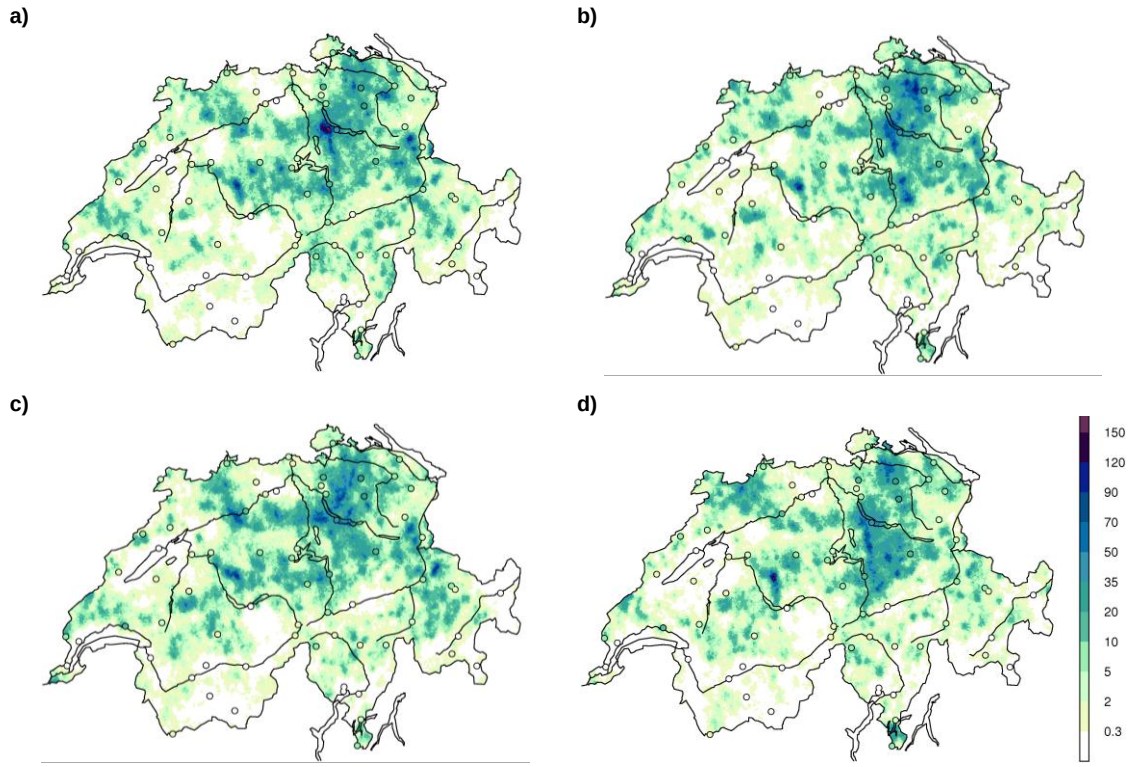

Figure 28 Four ensemble members from CSCOMB_smn on the 10 June 2008. Precipitation is given in mm.

Subtracting the trend from the precipitation fields, Figure 30 shows the simulated residual fields (i.e. the stochastic component of the underlying geostatistical model) in the transformed space. CSCOMB and CSGAU with both station densities all have a different trend field. As the residuals at gauge locations are computed from the difference between gauge observations and trend estimate at the same location, they depend on the trend field. We therefore cannot compare the locations of positive and negative values of the simulated residual field among the different methods. What we can compare are the spatial characteristics of the simulated residual fields.

The simulated residual fields from CSGAU show much more large-scale variation. Independent of the network density and the specific ensemble member, the residuals at gauge locations and thus the simulated residual fields are in general negative (i.e. the trend is corrected downwards) in the Valais and positive around the lake of Zurich. We expect this behavior, since the trend field from CSGAU corresponds to the mean of the gauge observations. The simulated residual field therefore corrects the trend upward in wet and downward in dry regions. With CSCOMB, this large-scale variation is in the form of the radar information already included in the trend field. The simulated residuals from CSCOMB therefore do not show this large-scale variation pattern.

Comparing the simulated residuals generated using the sparse and the dense station network, we again see the nugget effect causing a lot of small-scale variability in the simulated residual fields of CSCOMB_all and CSGAU_all. The nugget effect is more clearly visible if we consider the simulated residual field alone, i.e. without the additional trend. Having a nugget of zero in the original data, both CSCOMB_smn and CSGAU_smn do not show this small-scale variance.

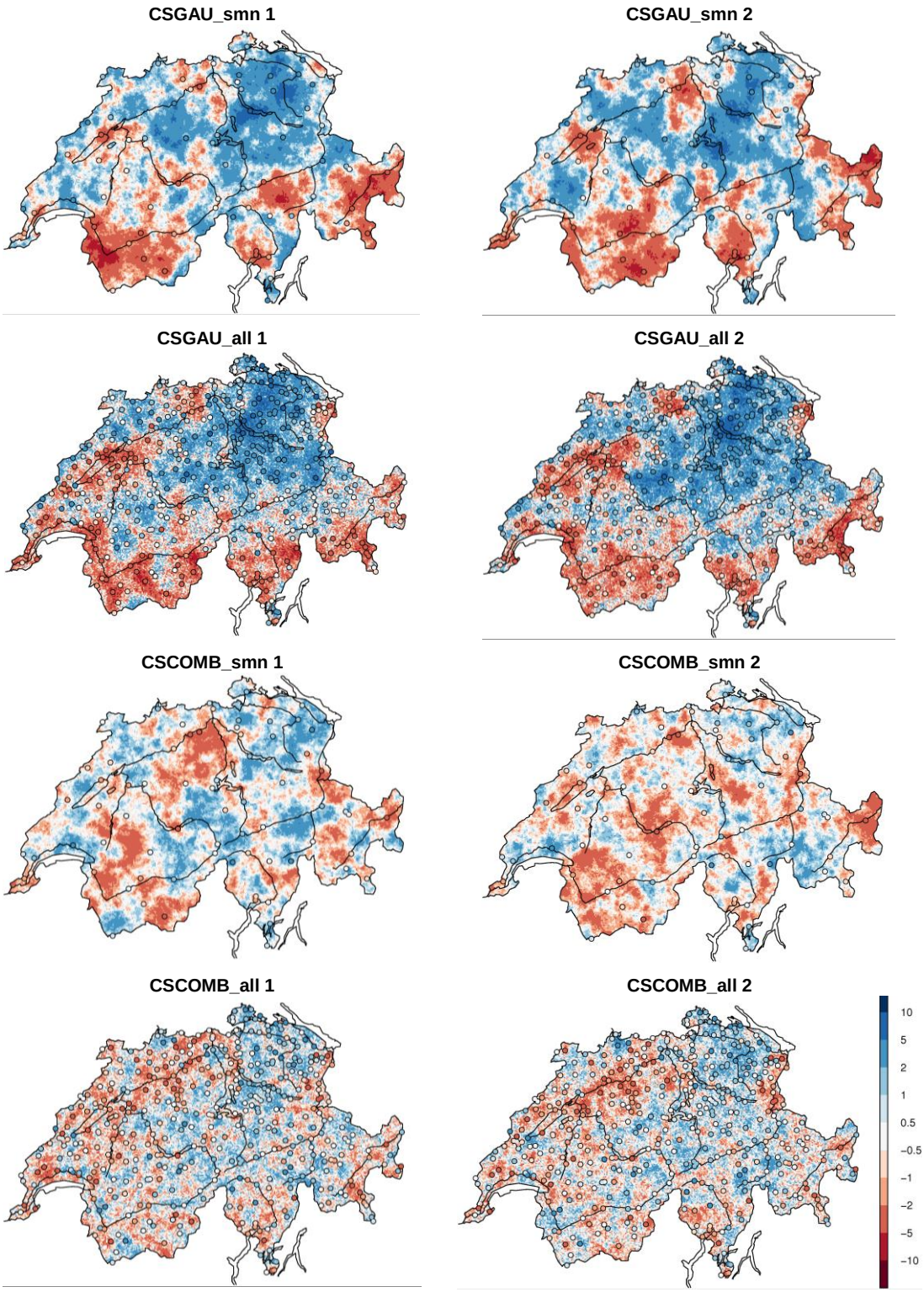

Figure 29 Two realizations of the simulated residual field in transformed space on the 10 June 2008 with CSGAU and CSCOMB for both network densities.

If we make the comparison between the two members of the same method, we see that they seem to differ more strongly for the sparse station network. The members of CSCOMB_all and CSGAU_all both show fairly similar simulated residual fields. We interpret this such that the uncertainty about the true precipitation field is smaller when the dense station network is used. Due to the strength of the small-scale variance, however, differences between members are hard to make out and we rather wait for section 6.3 to make statements regarding the uncertainty in the estimates.

The 8 August 2007 is our example day of stratiform precipitation. The day is characterized by large radar errors. This is reflected in the uniform trend fields of CSCOMB, very similar to the constant mean trend of CSGAU (not shown). The relatively large nugget observed manifests in the simulated precipitation fields, too. The question, whether a precipitation field with this strong small-scale variance meets the expectations about a stratiform precipitation field, is pending. The mentioned issues are illustrated and elaborated in detail in section B of the appendix.

The last example day to be discussed is the 6 September 2008. This day is characteristic for an overall convective precipitation situation with an intense local maximum of precipitation in the Ticino. With conditional simulation, the representation of this local maximum in the ensembles is worth a discussion. Moreover, the fate of the radar stripes visible in Figure 2 needs to be investigated. Details on the above are provided in section B of the appendix.

6.3 Experiments for quantifying the uncertainty reduction attributable to different method settings

The previous sections of this chapter highlight the differences of the three example days. Here we want to investigate how these differences condense quantitatively in the spread of the mean areal precipitation of the ensembles. The Reuss catchment is used for this quantification (see Figure 23). Before we dive into the different experiments, it should be noted that we just show examples and do not perform a systematic analysis here. This section rather serves to illustrate what opportunities conditional simulation offers than to claim representativeness. Nevertheless the results provide exemplary insight into the variation and dependency of estimation uncertainty and serves as a qualitative plausibility assessment of the simulation concept.

Figure 30 shows the relative spatial uncertainty (i.e. the estimated uncertainty in our model represented by the spread between the ensemble members) of the mean areal precipitation in ensembles of 100 members simulated with CSCOMB_smn. On all the example days, the spread between the ensemble members increases for decreasing catchment size. For intuition, a relative spread (i.e. the r.sd (equation (10)) normalized with the median; see Table 5) of 0.483 for Schaechenbach corresponds to an r.sd of 6.24 mm (at a median of 12.9 mm). This reduces to 2.379 mm (at a median of 11.84 mm) for the complete Reuss catchment. We expected to find a reduced spread of mean areal precipitation in larger catchments and interpret it as being caused by stronger compensation of the random deviations in catchments of bigger size.

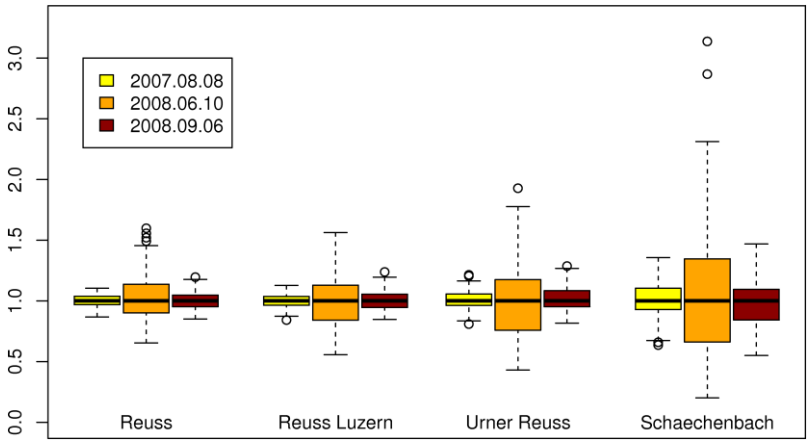

Figure 30 Boxplots of mean areal precipitation for the four catchments Reuss (3431 km^2), Reuss Luzern (2261 km^2), Urner Reuss (847 km^2) and Schaechenbach (106 km^2). Results from CSCOMB_smn with 100 ensemble members are shown for the three example days. The areal means are normalized with the median of the respective catchment and day.

The differences between the spread of the different days are considerable. The smallest spread is achieved on the 8 August 2007, the day with stratiform precipitation. Of the two convective days, the 6 September 2008 (overall convective precipitation) has a lower spread. We interpret the reduced spread in case of stratiform precipitation as caused by the higher spatial autocorrelation of the observations manifesting in the larger range (201 km compared to 35 km (10 June 2008) and 140 km (6 September 2008)). Furthermore, the average precipitation amount estimated on the example day of stratiform precipitation is higher (see Figure 2), which reduces the relative uncertainties. The spread between the ensemble members is highest on the day with isolated convective precipitation. We argue that both the average precipitation and the range are smallest on this day. Precipitation therefore co-varies only over short distances which increases the random spread. On the level of mean areal precipitation, the very small-scale and spatially uncorrelated nugget variance is compensated and thus, no nugget effect is observed.

From a certain catchment size on, a further increase in catchment size does not seem to reduce the spread any further. The 740 km^2 increase from the Schaechenbach to the Urner Reuss catchment reduces the spread in the areal means more strongly than the 1400 km^2 increase from Urner Reuss to Reuss Luzern. We would expect this behavior, since the relative increase in size is much bigger from Schaechenbach to Urner Reuss than from Urner Reuss to Reuss Luzern.

Table 5: Relative standard spread of mean areal precipitation of ensembles with 100 members for the four catchments Reuss, Reuss Luzern, Urner Reuss and Schaechenbach. The relative standard spread is defined as the r.sd normalized with the median of the respective catchment and method setting. Results from CSGAU and CSCOMB with both network densities are shown for the 10 June 2008.

	Reuss	Reuss Luzern	Urner Reuss	Schaechenbach
CSGAU_smn	0.253	0.267	0.360	0.671
CSGAU_all	0.107	0.136	0.262	0.294
CSCOMB_smn	0.201	0.223	0.285	0.483
CSCOMB _all	0.080	0.094	0.192	0.266

Concentrating on the 10 June 2008, Table 5 shows the relative r.sd of precipitation for the four catchments with CSCOMB and CSGAU for both network densities. The strongest uncertainty reduction is achieved with CSCOMB_all, followed by CSGAU_all and CSCOMB_smn. Most uncertainty regarding the true precipitation field is in simulations with CSGAU_smn. Bringing the results of the best estimates back into mind, we see that the improvement of the combination and the single-sensor reference with both network densities is similar for both the accuracy of the point estimates (kriging) and the spatial uncertainty in the ensembles (conditional simulation). First, 360 additional gauges are more successful in reducing the spatial uncertainty than the radar information. Second, CSCOMB reduces the spatial uncertainty compared to CSGAU with the same station network. Third, the additional radar information tends to reduce the spread more strongly if we use the sparse station network. The radar information in this example, hence, successfully reduces the spatial uncertainty of mean areal precipitation. These results demonstrate that our conditional simulation technique plausibly reproduce the uncertainty of the estimates.

Figure 31 illustrates the spread in the areal means for the different catchments with boxplots for all the example days. On top of the information from Table 5, we see in the boxplots that CSGAU tends to have more outliers than CSCOMB on the 10 June 2008. Especially CSCOMB_all seems to be outlier-free.

Looking at the 6 September 2008, we draw the same conclusions concerning the level of uncertainty in the simulated precipitation fields. CSCOMB_all exhibit the lowest and CSGAU_smn the highest uncertainty in the ensembles. CSCOMB_all has some outliers observed on this day, too. We interpret these outliers observed with CSCOMB and CSGAU with both network densities as a characteristic of conditional simulation to simulate both extremely low and extremely high precipitation.

On the 8 August 2007, the benefit of radar information is not apparent. The spread of CSCOMB is not systematically smaller than the spread of CSGAU. With the dense gauge network the simulated fields have lower spread than with the sparse SMN network. This result is indicated by the low βs (see Figure 2) on this day. We suggest, again, radar information to be particularly beneficial in case of convective precipitation. Whereas for stratiform (spatially more coherent) precipitation patterns, a dense gauge network is more decisive for estimating catchment mean precipitation.

In section 6.1 the differences between the ensemble and kriging standard spread are analyzed. We saw that many realizations are required to approach the theoretical model spread (i.e. the kriging spread) by the ensembles. Here we undertake an experiment to examine the sensitivity with respect to ensemble size of catchment mean precipitation. Results are shown in Figure 32. We see that the spread varies with different ensemble sizes. The spread confined by the whiskers of the boxplot increases for increasing ensemble sizes in both catchments. Yet, interquartile range (i.e. the size of the box) for Reuss Luzern is overestimated in small ensembles and remains constant for ensembles with 100 and more members. On the contrary, the interquartile range increases from 10 to more ensemble members for the Schaechenbach catchment. The really extreme precipitation (represented by the outliers) only becomes abundant in ensembles with more than 100 members. This is due to the better sampling of the skew pdf. The outliers with extremely low precipitation are missing. Since we saw ensemble members with extremely low precipitation represented in Figure 31, we do not expect the issue to be systematic.

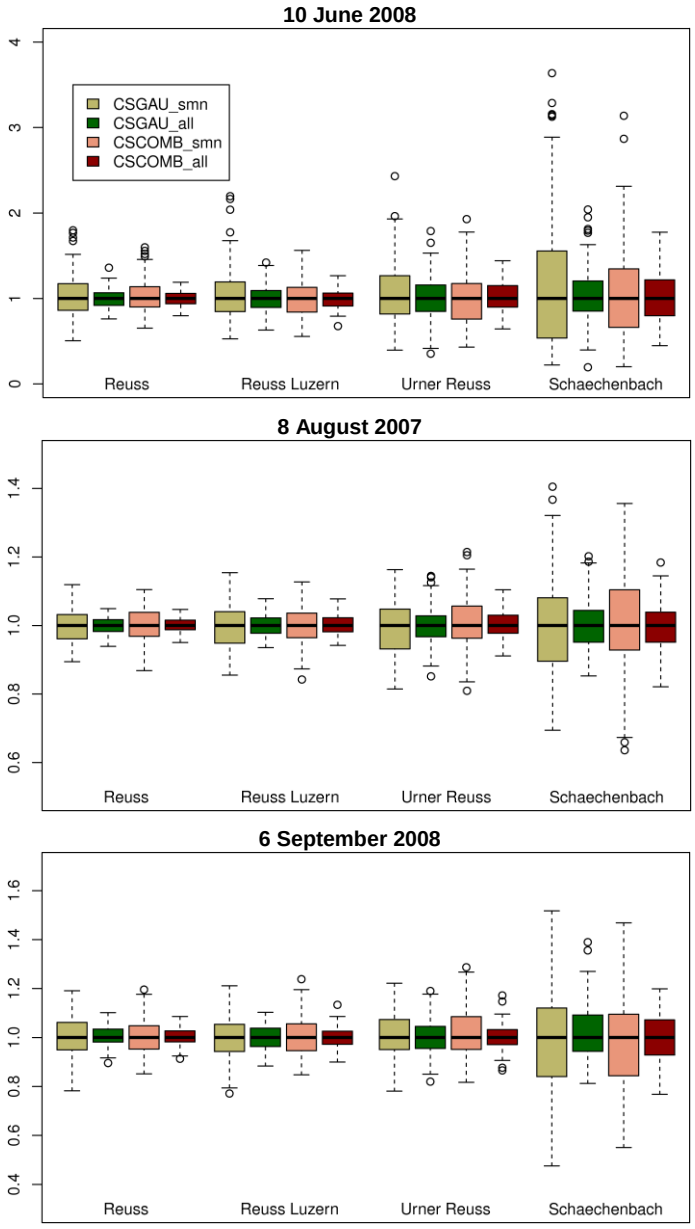

Figure 31 Boxplots of areal mean precipitation for the four catchments Reuss, Reuss Luzern, Urner Reuss and Schaechenbach on the three example days. Results from CSGAU and CSCOMB with both network densities with 100 ensemble members are shown. The areal means were normalized with the median of the respective catchment, day and method setting. Note that the scale changes for the different days.

We would expect the spread of the larger catchment (Reuss Luzern) to be well approached with fewer simulations than it is the case for the smaller catchment (Schaechenbach). Indeed, the spread seems not to vary too much for increasing ensemble sizes in the larger catchment. For extreme values to be simulated, however, it still needs more than 200 ensemble members. Since results from one single experiment are presented, a generalization of these findings is difficult. Nevertheless, considering that this convective case represents more demanding conditions, a minimum of 100 members is a reasonable requirement for catchment sizes larger than 100 km^2.

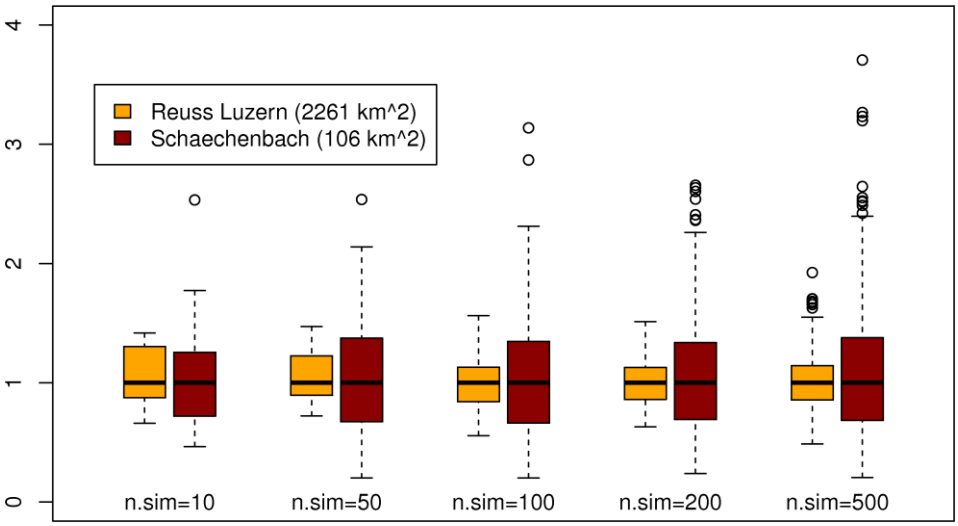

Figure 32 Boxplots of areal mean precipitation for the two catchments Reuss Luzern and Schaechenbach on the 10 June 2008. Results from CSGAU_smn with 10, 50, 100, 200 and 500 ensemble members are shown. The areal means were normalized with the median of the respective catchment and ensemble size.

Up to now, we only considered precipitation on the daily time scale in this plausibility assessment. Figure 34 shows how the aggregation of daily precipitation fields over a whole month reduces the uncertainty in the precipitation estimates. With the monthly aggregation, the spread observed in the daily estimates is reduced. We would expect this behavior, since the increased time scale over which the simulated precipitation fields are aggregated is suggested to have a similar effect as the increased area over which precipitation is averaged. As the ensemble members are temporally independent, random daily deviations compensate each other in a monthly aggregation. We did not perform a systematic analysis of the influence of the time scale though. The comparison here is made between arbitrary example months and days. No interpretation on the magnitude of the uncertainty reduction from the increased time scale can be provided.

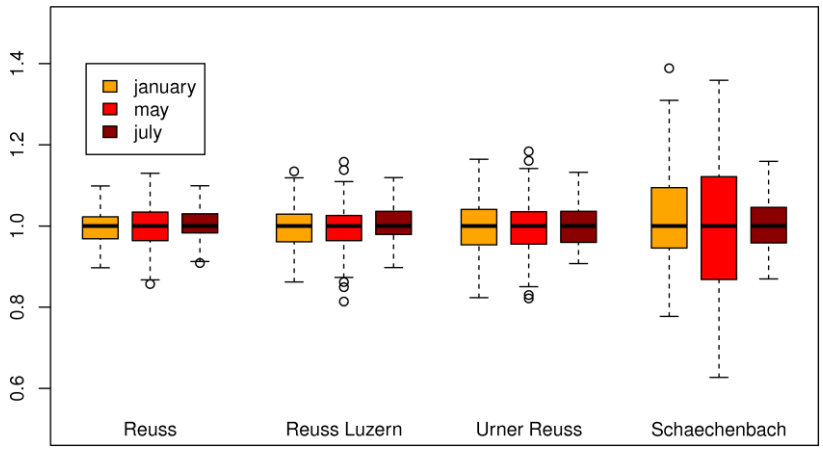

Figure 33 Boxplots of areal mean precipitation for the four catchments Reuss, Reuss Luzern, Urner Reuss and Schaechenbach on the three example months January, May and July 2008. Results from CSGAU_smn with 100 ensemble members are shown. The areal means were normalized with the median of the respective catchment and month.

If we compare the spread of the different catchments, we see that the spread is biggest in the Schaechenbach catchment with an uncertainty of 10 - 20% (interquartile range) depending on the considered month. The three larger catchments have much smaller and more similar spreads. Also the difference between the three months is biggest for the Schaechenbach catchment. We argue that an aggregation over 31 days cannot compensate the strong random deviations observed in such a small catchment.

The month May 2008 has the biggest spread for the Schaechenbach catchment and more outliers than the other two months. May 2008 is an example of a month where a few days of intensive precipitation made up for most of the precipitation fallen during the entire month. We therefore suggest the increased spread to be caused by the relatively strong influence of the uncertainty of the days with very intense precipitation, preventing a strong compensation of random daily deviations by the monthly aggregation. The two other months have a more uniform distribution of precipitation among the individual days of the month.

7 Conclusions

In this thesis we have investigated a statistical technique of radar-gauge combination to produce precipitation estimates in Switzerland that include measures of the pertinent analysis uncertainty. The methodology builds on a geostatistical simulation framework, which delivers an ensemble of precipitation fields that are all consistent with the measurements (conditional simulation). Compared to the conventional target of one 'best estimate', the ensemble technique provides a fully probabilistic estimate of the observed precipitation distribution. This is particularly suitable in applications that require realistic spatial structures in precipitation fields and where the consideration of uncertainties is crucial (e.g. in runoff modeling). The thesis has focused on daily precipitation totals in Switzerland. It has thoroughly evaluated the geostatistical methodology (kriging with external drift; KED), assessed the reliability of the ensembles, and examined sensitivities with respect to the rain gauge network density.

The combination represents a substantial improvement over precipitation estimates from more traditional single-sensor methods. The accuracy of the rain gauge measurements and the high resolution of the radar information are successfully brought together. The systematic bias is strongly reduced compared to the radar reference. In particular, the strong geographic bias due to underestimation in the mountainous regions and overestimation in the Swiss Plateau is removed. The combination shows particular skill when it comes to distinguishing wet and dry areas. In convective precipitation situations the benefit of the additional radar information is specifically strong: the skill measures of the combination are particularly high in summer, when convective precipitation is abundant. The combination used is able to both take advantage of the radar information when it is beneficial and avoid potential negative influences when radar information is erroneous. Similar results were found in comparable studies using the same combination technique in Switzerland for a case study of daily precipitation (Erdin, 2009) and a systematic analysis of hourly precipitation (Keller, 2012). The results are in line with a study by Schuurmans et al. (2007) that found KED to produce more accurate daily precipitation estimates than single-sensor methods. Goudenhoofdt and Delobbe (2009) also find radar benefits to be particularly significant in summer.

As in Erdin (2009), the added value of the combination is sensitive to the rain gauge network density. The increase in skill of the combination over a rain gauge only reference is twice as high when the sparse SMN network is used. Since the automatic SMN stations have a ten minute time resolution, the combination is particularly interesting on short time scales and in real-time applications. Another feature where the combination improved the quality of the best estimates is the representation of intense precipitation. Precipitation exceeding predefined thresholds is less often classified as extremely unlikely by the cross-validated probabilistic estimate of the combination. This signalizes a better representation of intense precipitation by the combination, which is useful in applications of conditional simulation.

A particularly interesting finding is that greater improvement in the quality of the best estimates can be achieved through additional information from the 366 climatological gauges, rather than from radar data. The skill and the reliability of the precipitation estimates are systematically higher when the dense gauge network is used. This is an important result of the systematic evaluation. In a first

case study restricted to five example days (Erdin, 2009), adding radar information to a sparse gauge network was found to be more beneficial compared to adding information from a denser gauge network. Also Haberlandt (2007) find the addition of radar information to hourly precipitation observations from 21 automatic gauges to be more important than additional information of 281 climatological gauges on the total rainfall sum of a four day flood event in Germany. Unfortunately, a comparison of our results to Haberlandt (2007) is possible only to a limited extent. Information from the climatological gauges cannot be used one-to-one on the hourly time scale and radar data quality in Switzerland suffers from the shadowing of mountains, unlike in Germany.

Illustrative example cases demonstrate that the conditional simulation technique can plausibly deal with the uncertainties in the estimates. The variations and dependencies of the estimation uncertainty are plausibly reproduced in the simulated ensembles. Additional information from a denser rain gauge network, for example, leads to a stronger reduction of the pertinent uncertainty. Also the additional radar information in the combination and both spatial and temporal aggregation reduce the uncertainty in the precipitation estimates. An issue worth discussing is the number of simulations to be performed in order to represent the theoretical model spread (inferred by the kriging standard spread) adequately. We could show that for a good representation of both theoretical spread and extremes at single grid points, at least 100 ensemble members are needed. Previous studies use ensemble sizes of 25 (Germann et al., 2009), 40 (Ekström et al., 2007) or 100 members (Ahrens and Jaun, 2007). Here it appears that ensembles with less than 100 members cannot properly reflect the theoretical model spread. Yet, the plausibility assessment indicates the required ensemble size to be sensitive to spatial aggregation and the precipitation situation. In small catchments it thus requires ensembles of bigger size to adequately reproduce the theoretical model spread.

Our combination approach incorporates two major limitations. First, we assume the rain gauges to represent the correct value of precipitation at their respective locations. Both the rain gauge and the radar observations, however, are uncertain. Second, the rain gauge observations are point measurements, whereas the radar data and, finally, the gridded estimates refer to areal precipitation of 1 km^2. This induces problems of scale compatibility in the combination of radar and gauge data. We therefore have to be aware that the real uncertainty of precipitation is different or rather higher than the uncertainty captured in the model.

The presented combination delivers best estimates and ensembles with limited precision. The precision can be improved either through advances regarding the observational monitoring system or by methodological developments. MeteoSwiss is undertaking efforts to reduce limitations of the observational monitoring system. The density of the automatic gauge network is being increased, two more radars in the Grisons and the Valais are to be installed and the measurement technology upgraded (MeteoSwiss, 2012; MeteoSwiss, 2010). Concerning methodological developments, we can think of a number of potential improvements that could be achieved in further investigations. The regional differences in the quality and the reliability of the estimates are considerable. We have to raise the question whether the stationarity assumption for the whole territory of Switzerland can be maintained. Our main argument for a stationarity assumption is the limited availability of observations and potential robustness problems induced by a small sample. Especially with the climatological gauge network and in the light of the denser SMN network, region-specific stationarity assumptions should be examined. Moreover, the strong regional differences in the Bias motivate an investigation of potential benefits of a regionally varying trend. Thereby, the influence of regions with particularly

large radar errors, like Western Switzerland on the 8 August 2007, might be reduced. Since the radar artifacts could not be entirely removed in the combination, an inclusion of information about radar quality is appealing. Erdin (2009) attempted to add a radar uncertainty term to the model. Though unsuccessful, they suggest that a more sophisticated modeling technique should lead to model improvement. We consider a principal component analysis of radar errors as a potential candidate for this. As in Keller (2012) and Erdin (2009), radar information is found to be particularly beneficial for distinguishing between wet and dry areas. This could possibly be exploited by indicator kriging with radar information used to indicate wet and dry regions, as done by Schleiss et al. (2012).

In contrast to conditional simulation, a series of previous studies was performed using KED and related kriging techniques in the radar-gauge merging context at MeteoSwiss (e.g. Erdin et al., 2012; Erdin, 2009; Keller, 2012; Sideris, submitted). Moreover, a combination method is already operational (Sideris et al., submitted). An open issue is the W-shape of the reliability plots produced on the daily time scale. The increase in relative frequencies around the median was not observed for hourly precipitation. A comparison of the hourly and the daily radar-gauge combination product would be valuable. Due to the longer aggregation period, days requiring a fall-back solution for parameter estimation are rarer. In the application with the dense gauge network, the variogram and model parameters are thus expected to be estimated more reliably.

In this first attempt to apply conditional simulation in a radar-gauge merging context, we performed a case study of three example days characterized by different precipitation situations. First results are promising and indicate potential for further investigations. We propose to study more example days to learn about other interesting features of conditional simulation. An investigation of the behavior of the ensemble spread with the dense station network and the single-sensor reference could be worthwhile. We just perform conditional simulation with a rain gauge only reference. It would be interesting to compare the combined ensembles to a single-sensor ensemble from radar. The implemented procedure of conditional simulation yields arrays of point values rather than areal averages of grid pixels. For a further development of our simulation procedure to simulate grid pixel averages, we can think of two interesting options. First, grid pixel averages could be created by simulating on a high resolution grid (say on a 4x4 pixel subgrid for every pixel of the original grid) and subsequent averaging to the coarser grid. Second, block kriging provides an interesting framework to simulate block values instead of point values.

The generated observation ensembles could be used for designing the monitoring and warning systems. Where the spatial uncertainty of precipitation is high, additional measurement stations are particularly necessary. A possibility to validate the spatial uncertainty in the simulated precipitation fields is to feed them into a hydrological rainfall-runoff model (e.g., Germann et al., 2009; Zappa et al., 2008). This allows for a comparison of both the spread of simulated mean areal precipitation with the spread of the simulated runoff, and a comparison of the simulated to the observed river runoff. Although the results are affected by the quality of the hydrological model too, a real world verification of the spatial uncertainty in the estimates is possible. For example, an investigation of the ability of the simulated ensembles to forecast river runoff during the heavy precipitation event in August 2005 could provide valuable insight into the performance of conditional simulation in the radar-gauge merging context.

Emery and Lantuéjoul (2006) mention limitations of the R-package used for simulation, causing inefficiencies when covariances are not smooth at the origin or leading to a loss in accuracy of the covariance reproduction. The technical verification performed shows the simulated precipitation fields to meet the requirements. Still, the different simulation algorithms implemented in the R-package RandomFields (e.g., turning bands methods or circulant embedding; see Schlather (2001)) motivate an investigation whether specific simulation algorithms are advantageous in our framework.

Abbreviations

ALL	Station network including both automatic SMN and climatological gauges
Bias	Systematic error computed on logarithmic scale; skill measure
C()	Covariance function
C(0)	Total variance (i.e. $\sigma^2_n + \sigma^2_{ps}$)
CSCOMB	Conditional simulation from combined radar-gauge data
CSCOMB_smn	CSCOMB using gauge observations from the SMN station network
CSCOMB_all	CSCOMB using gauge observations from the station network ALL
CSGAU	Conditional simulation from rain gauge data; single-sensor reference method
CSGAU_smn	CSGAU using gauge observations from the SMN station network
CSGAU_all	CSGAU using gauge observations from the station network ALL
E	Matrix with the eigenvectors in the columns
e_k	Eigenvector
est	Estimation
h	Lag; Euclidean distance between two points
HK	Hanssen-Kuipers discriminant; skill measure
i, j	Indices for spatial reference
KED	Kriging with external drift
KED_smn	KED using gauge observations from the SMN station network
KED_all	KED using gauge observations from the station network ALL
MAD	Mean absolute deviation; skill measure
MLE	Maximum likelihood estimation
obs	Observation
OKGAU	Ordinary Kriging of rain gauges; single-sensor reference method

OKGAU_smn	OKGAU using gauge observations from the SMN station network
OKGAU_all	OKGAU using gauge observations from the station network ALL
P	Modeled precipitation amount
pdf	Probability density function
QPE	Quantitative precipitation estimate
Q	Quantile
r	Range parameter corresponding to 1/3 of the practical range
RADAR	QPE product from radar; single-sensor reference method
r.sd	Robust spread measure
Rel. MRTE	Relative mean root transformed error; skill measure
REML	Restricted maximum likelihood estimation
RHIRES	Deterministic spatial interpolation method
S	Variance
SCATTER	Skill measure
SEEPS	Stable equitable error in probability space; skill measure
SMN	SwissMetNet; automatic station network
Y	Untransformed precipitation data
Y*	Transformed precipitation data
x	Simulated random vectors
Z	Random process or radar reflectivity, depending on the context
α	Intercept of linear trend model
β	Trend coefficient of linear trend model
γ()	Variogram
λ	Transformation parameter or eigenvalue; depending on the context
λ_{lower}	Lower bound of the transformation parameter λ
Σ	Covariance matrix
σ^2_n	Nugget
σ^2_{ps}	Partial sill

References

Ahrens, B.; Jaun, S. (2007), 'On evaluation of ensemble precipitation forecasts with observation based ensembles', *Adv. Geosci.* **10**, 139–144.

Box, G. E. P.; Cox, D. R. (1964), 'An analysis of transformations', *J. Roy. Stat. Soc.*, **26A**, 211-252.

Clark. M. P.; Slater, A. G. (2006), 'Probabilistic quantitative precipitation estimation in complex terrain', *J. Hydrometeorol.* **7**, 3–22.

Cressie, N.A.C. (1993), 'Statistics for Spatial Data', *Wiley*, Chichester, 900 pp.

DeGaetano, A. T.; Wilks, D. S. (2008), 'Radar-guided interpolation of climatological precipitation data', *Int. J. Climatol.* **29**, 185–196, doi:10.1002/joc.1714.

Ekström, M.; Kyriakidis, P. C.; Chappell, A. (2007), 'Spatiotemporal Stochastic Simulation of Monthly Rainfall Patterns in the United Kingdom (1980–87)', *J. Climate* **20 (16)**, 4194-4210.

Emery, X., Lantuéjoul, C. (2006), 'TBSIM: a computer program for conditional simulation of three-dimensional Gaussian random fields via the turning bands method', *Comput. Geosci.* **32 (10)**, 1615-1628.

Erdin, R; Frei, C.; Künsch, H. R. (2012), 'Data transformation and uncertainty in geostatistical combination of radar and rain gauges', *J. Hydrol.* **13**, 1332-1346.

Erdin, R. (2011), 'Evaluation guidelines of CombiPrecip', Internal report, MeteoSwiss, 10pp.

Erdin, R. (2009), 'Combining Rain Gauge and Radar Measurements of a Heavy Precipitation Event over Switzerland', Veroeffentlichungen der MeteoSchweiz 81, 108 pp.

Frei, C.; Germann, U.; Fukutome, S.;Liniger, M. (2008), 'Möglichkeiten und Grenzen der Niederschlagsanalysen zum Hochwasser 2005', Arbeitsberichte der MeteoSchweiz 221, 19 pp.

Frei, C.; Schöll, R.; Fukutome, S.; Schmidli, J.; Vidale, P.L. (2006), 'Future change of precipitation extremes in Europe: An intercomparison of scenarios from regional climate models', *J. Geophys. Res.* **111**, D06105, doi:10.1029/2005JD005965.

Frei, C.; Schär, C. (1998), 'A precipitation climatology of the Alps from high-resolution rain-gauge observations', *Int. J. Climatol.* **18**, 873-900.

Germann, U.; Berenguer, M.; Sempere-Torres, D.; Zappa, M. (2009), 'REAL – Ensemble radar precipitation estimation for hydrology in a mountainous region', *Q. J. R. Meteorol. Soc.* **135**, 445–456.

Germann, U.; Galli, G.; Boscacci, M.;Bolliger, M. (2006), 'Radar precipitation measurement in a mountainous region', *Q. J. R. Meteorol. Soc.* **132**, 1669-1692.

Goovaerts, P. (1997), 'Geostatistics for Natural Resources Evaluation', *Oxford University Press*, New York, 483 pp.

Goudenhoofdt, E.; Delobbe, L. (2009), 'Evaluation of radar-gauge merging methods for quantitative precipitation estimates', *Hydrol. Earth Syst. Sci.* **13**, 195–203.

Haberlandt, U. (2007), 'Geostatistical interpolation of hourly precipitation from rain gauges and radar for a large-scale extreme rainfall event', *J. Hydrol.* **332**, 144-157.

Keller, D. (2012), 'Evaluation and comparison of radar-rain gauge combination methods-Scientific basis for selecting a new real-time precipitation estimation method for Switzerland', *Scientific Report MeteoSwiss* **94,** 80 pp.

Krajewski, W. F. (1987), 'Cokriging radar-rainfall and rain gage data', *J. Geophys. Res*. **92**, 9571-9580.

Lantuéjoul, C. (2002), 'Geostatistical Simulation. Models and Algorithms', *Springer*, Berlin, 256 pp.

Leuenberger, D., Rossa, A. (2007), 'Revisiting the latent heat nudging scheme for the rainfall assimilation of a simulated convective storm', *Meteor. Atmos. Phys.* **98**, 195–215.

MeteoSwiss (2012), 'Annual Report 2011', Federal Office of Meteorology and Climatology MeteoSwiss, 40 pp.

MeteoSwiss (2010), 'An observation network for the future', Federal Office of Meteorology and Climatology MeteoSwiss, 7 pp.

R Development Core Team (2011), 'R: A language and environment for statistical computing', R Foundation for Statistical Computing, Vienna, Austria, ISBN 3-900051-07-0, URL www.Rproject.org.

Rakovec, O.; Hazenberg, P.; Torfs, P. J. J. F.; Weerts, A. H.; Uijlenhoet, R. (2012), 'Generating spatial precipitation ensembles: impact of temporal correlation structure', *Hydrol. Earth Syst. Sci.* **16**, 3419–3434.

Ribeiro Jr., P.J.; Diggle, P.J. (2001), 'geoR: A package for geostatistical analysis', R-NEWS **1 (2)**, 15-18. ISSN 16093631.

Rodwell, M. J.; Richardson, D. S.; Hewson, T. D.; Haiden, T. (2010), 'A new equitable score for verifying precipitation in numerical weather prediction', *Q. J. R. Meteorol. Soc.* **136**, 1344-1363.

Seo, D.-J. (1998), 'Real-time estimation of rainfall fields using radar rainfall and rain gage data', *J. Hydrol*. **208**, 37-52.

Scherrer, S. C.; Frei, C.; Croci-Maspoli, M.; Van Geijtenbeek, D.; Hotz, C.; Appenzeller, C. (2011), 'Operational quality control of daily precipitation using spatio-climatological plausibility testing', *Meteorol. Z.* **20 (4)**, 1-11.

Schlather, M. (2001), 'Simulation of stationary and isotropic random fields', R-News, **1 (2)**, 18-20.

Schleiss, M.; Jaffrain, J.; Berne, A. (2012), 'Stochastic Simulation of Intermittent DSD Fields in Time', *J. of Hydrometeorol.* **13**, 621-637.

Schuurmans, J. M.; Bierkens, M. F. P.; Pebesma, E. J.; Uijlenhoet, R. (2007), 'Automatic Prediction of High-Resolution Daily Rainfall Fields for Multiple Extents: The Potential of Operational Radar', *J. Hydrometeorol.* **8**, 1204–1224.

Sevruk, B. (1985), 'Correction of precipitation measurements, summary report', *Proceedings of the* ETH:IAHS:WMO Workshop on the Correction of Precipitation Data, 13–23.

Sideris, I., Gabella, M.; Erdin, R.; Germann, U. (submitted), 'Real-time radar-raingauge merging using spatiotemporal co-kriging with external drift in the alpine terrain of Switzerland', *Q. J. R. Meteorol. Soc*.

Talagrand, O.; Vautard, R., Strauss, R. (1997), 'Evaluation of probabilistic prediction systems', Proc. ECMWF Workshop on Predictability, Shinfield Park, United Kingdom, ECMWF, 1–25.

Webster, R.; Oliver, M. A. (2007), 'Geostatistics for Environmental Scientists', *Wiley*, Chichester, 315 pp.

Viviroli, D.; Mittelbach, H.; Gurtz, J.; Weingartner, R. (2009), 'Continuous simulation for flood estimation in ungauged mesoscale catchments of Switzerland – Part II: Parameter regionalisation and flood estimation results', *J. Hydrol.* **377**, 208–225.

Wilks, D. (2006), 'Statistical Methods in the Atmospheric Sciences', *Elsevier*, Amsterdam, 627 pp.

Young, C.; Bradley, A.; Krajewski, W.; Kruger, A.; Morrissey, M. (2000), 'Evaluating NEXRAD multisensor precipitation estimates for operational hydrologic forecasting', *J. Hydrometeor.* **1**, 241–254.

Zappa, M., and Coauthors (2008), 'MAP D-PHASE: Real-time demonstration of hydrological ensemble prediction systems', *Atmos. Sci. Lett.* **9**, 80–87.

Acknowledgement

With all due thunder and fanfare I would like to express many thanks to my supervisors. I want to thank Christoph Frei for passing on the knowledge and enthusiasm for spatial climate analysis. The sudden speed up of progress after Rebekka Erdin joined the team is the best proof of her valuable support. The meetings we had were always very motivating and fruitful.

I am grateful to Sophie Fukutome and Bettina Weibel – for sharing the office, the kettle, the English language expertise and the wisdom that 'es bizeli fürschi mache' is always good. David Masson introduced me to the CSCS resources and provided initial support, what I greatly appreciate. I am thankful to Mark Liniger for providing all the resources needed for this project. Special thanks go to all APK members: I greatly enjoyed the inspiring breaks on the roof top overseeing all Zurich.

More thanks go to the unknown person of the R community feeding all the forums and help pages with valuable hints.

A Comparison of ensemble and kriging spread

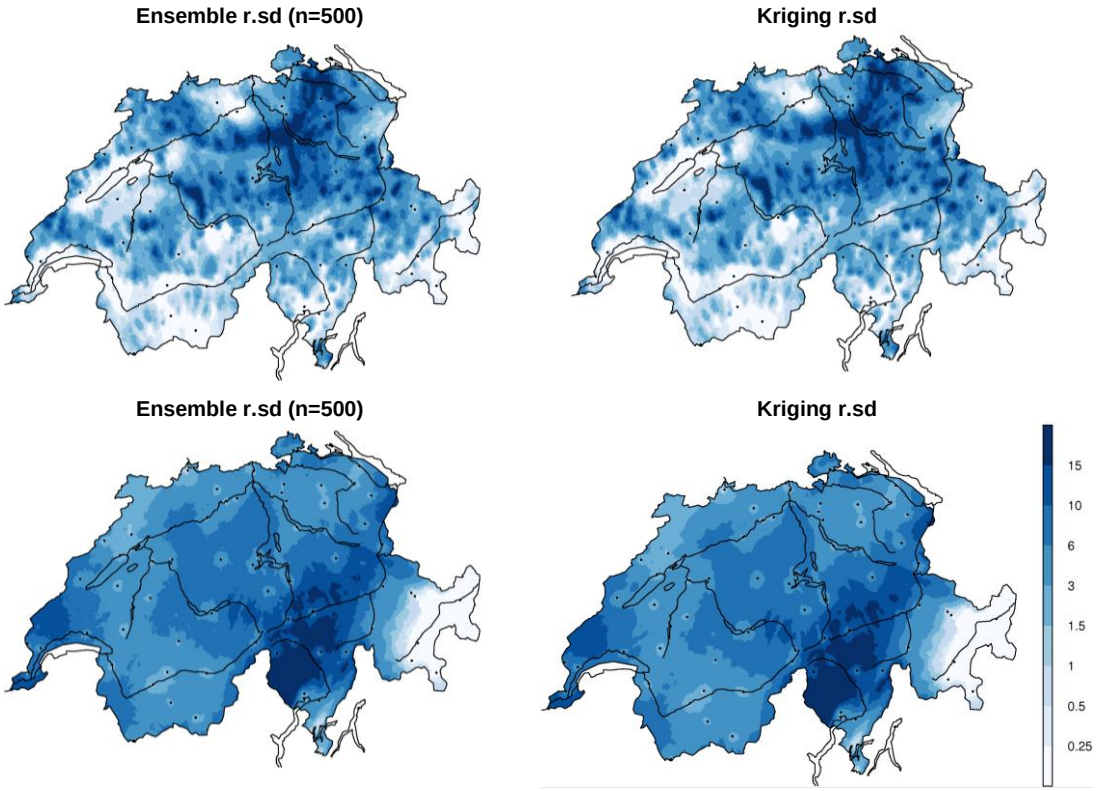

Figure A1 Ensemble r.sd from CSCOMB_smn for ensembles of 500 members and kriging r.sd from KED_smn on the 10 June (top) and the 6 September 2008 (bottom) in mm. The robust spread measure r.sd is defined in equation (10). See Figure 2 for an illustration of the precipitation situation on these days.

Similar to section 6.1, we analyze the standard spread of the ensembles and compare it to the theoretical model spread (inferred from the kriging standard spread) for the 10 June and the 6 September 2008. The small-scale variance in the spread is reduced compared to the 8 August 2007 on both convective days (Figure A1 and A2). Since the nugget of both days is zero, no nugget effect is observed. The spread in general, however, is less uniform. We therefore see more distinct maxima and minima of the differences of kriging and ensemble r.sd (Figure A2). The differences are especially low e.g. in the Valais (10 June 2008) and the eastern Grisons (6 September 2008). In these regions of weak precipitation, positive and negative differences between the ensemble and kriging r.sd are random. Where precipitation is intense, the theoretical spread is generally

underestimated by the ensembles. An example for this is the red area of strong underestimation in the Ticino on the 6 September 2008. We suggest these underestimations to be caused by the skewness of the precipitation distribution. If the very extreme values are coincidentally not realized, the theoretical spread is underestimated. The lower estimated λs (see Figure 2) of the two convective days indicate stronger skewness of the precipitation distribution. We therefore expect the described effect of underestimating the theoretical spread where precipitation is intense to be particularly strong on the convective days. With a very small ensemble, however, the model spread has a tendency to be underestimated also on the 8 August 2007. The negative differences in Figure 26 for the ensemble of 10 members are predominant. The skewness of the precipitation distribution, hence, seems to have a certain influence on the ensemble size required for a good representation of the theoretical model spread. On days where a strong transformation has to be applied to the data (i.e. very skew precipitation distribution and therefore small λs), the spread of the ensembles has a tendency to underestimate the theoretical spread where precipitation is intense.

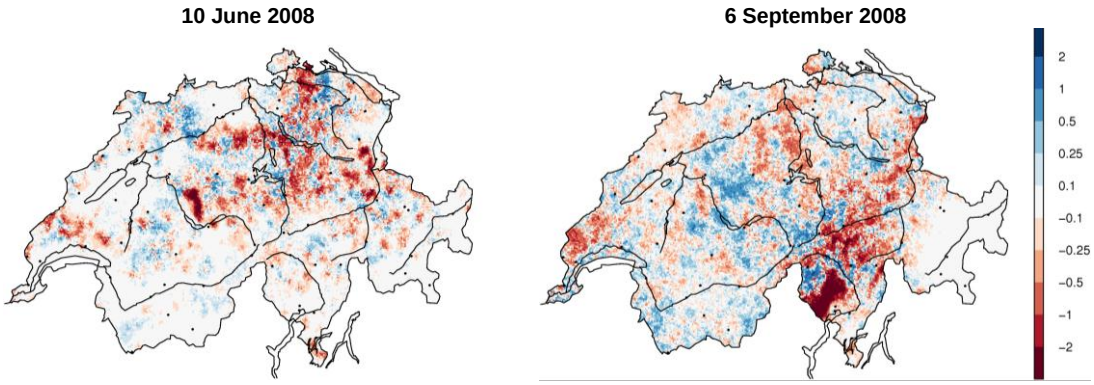

Figure A2 Differences between the ensemble and kriging r.sd for ensembles of 500 members on the 10 June and the 6 September 2008 in mm.

B Precipitation fields from conditional simulation

Best estimates and simulated realizations of precipitation for the combination and the single-sensor reference method with both station densities are shown in Figure B1 for the 8 August 2007. We find supported what we discussed in section 6.2 for the 10 June 2008: the simulated ensemble members represent the spatial variability of precipitation much better than the best estimates. The qualitative differences from OKGAU to CSGAU and from KED to CSCOMB are yet smaller. As pointed out in section 4.2.3, we suggest radar to be particularly beneficial in case of convective precipitation. The radar benefit does not seem to be given in case of the stratiform precipitation occurring on the 8

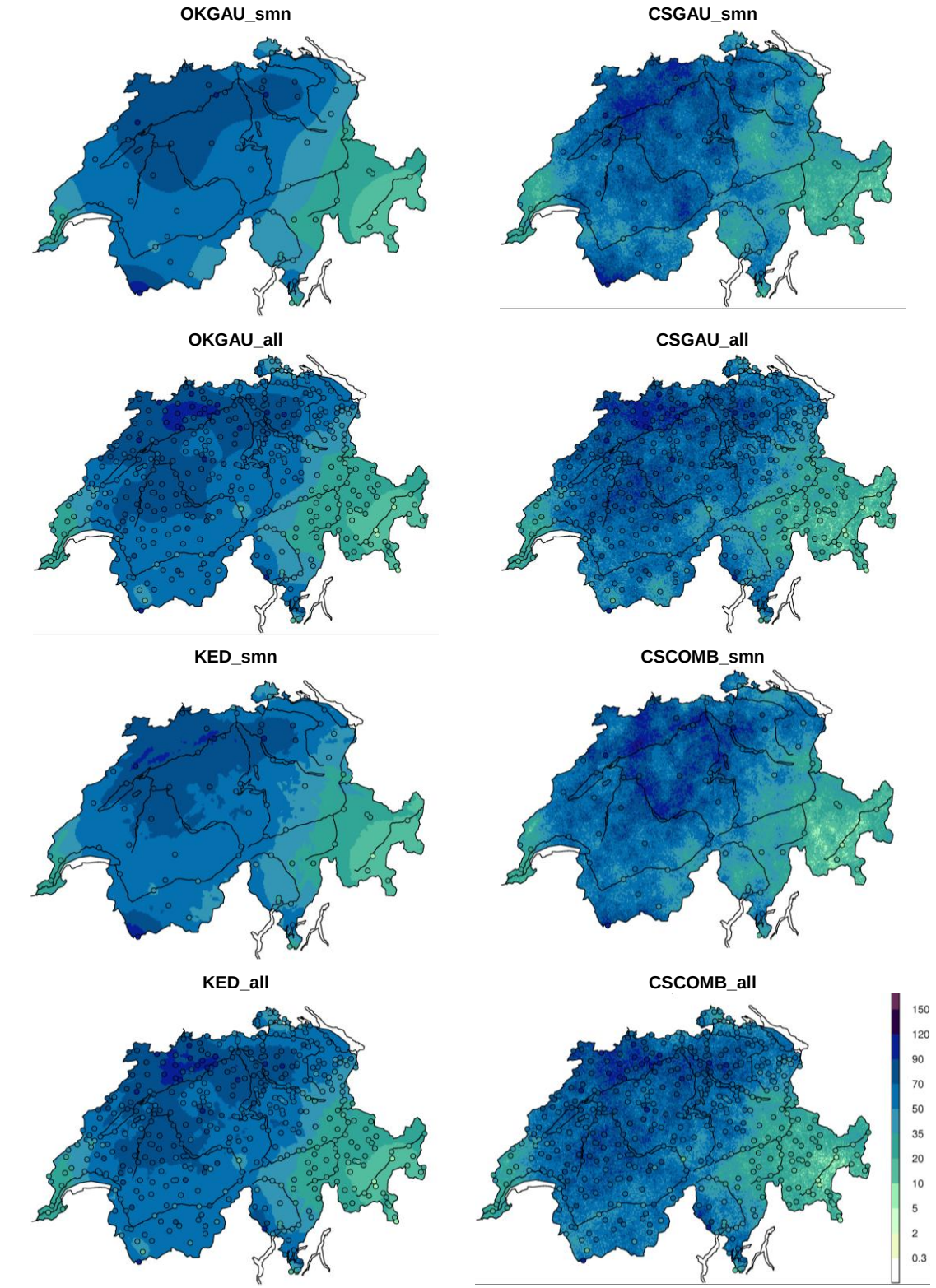

Figure B1 Best estimate fields of precipitation from kriging (left) and one ensemble member from conditional simulation (right) on the 8 August 2007 in mm. Precipitation fields are shown for the single-sensor reference method (OKGAU and CSGAU) and the combination method (KED and CSCOMB) for both network densities.

August 2007. Here, the quality of the additional radar information is low due to large radar errors (especially in Western Switzerland). This manifests in the particularly low radar coefficient β (see Figure 2 for a list of estimated βs on the example days). The βs on the example days of convective precipitation are more than twice as high as the βs on the 8 August 2007. There is thus low trust in the radar information here and the trend field of the combination, in contrast to the 10 June 2008, cannot capture the variability in the data. If we compare fields of simulated residuals from CSCOMB_smn and CSGAU_smn (see Figure B2), we find similar large-scale variation patterns. Negative residuals are predominantly simulated in the east and the far west, positive residuals in between. The trend fields of both CSGAU_smn and CSCOMB_smn therefore experience comparable correction by the simulated residual fields.

On the 8 August 2007, all the precipitation fields from conditional simulation have a lot of small-scale variance. We again argue with the nugget-to-sill ratio which is between 0.05 and 0.13 for CSCOMB and CSGAU with both network densities. What can be seen here is the ability of conditional simulation to represent extreme values. One automatic and three climatological gauges in the Grisons observe less intense precipitation than the surrounding gauges. Whilst the information of these gauges does not seem to be reflected in the best estimates, it is represented in the simulated precipitation fields. The uncertainty with respect to the true field accounted for in the geostatistical model allows the simulation of very low precipitation amounts.

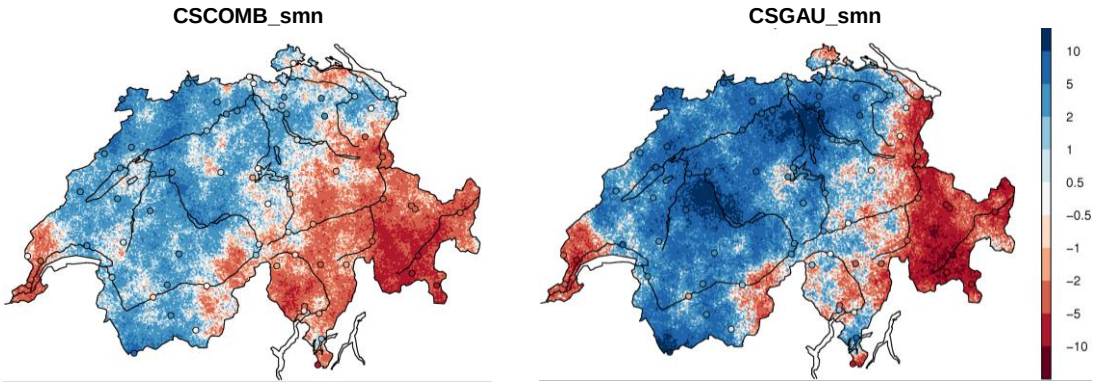

Figure B2 Realizations of the simulated residual field from CSCOMB_smn and CSGAU_smn in transformed space on the 8 August 2007.

Would we expect so much small-scale variability in the Swiss Plateau in the case of stratiform precipitation? Concerning stratiform precipitation, measurement errors at gauges are from experience relatively small. There are, however, many different factors influencing precipitation. We could imagine the small-scale variance in the original data to be predominantly caused by gauges located in mountainous regions, where small lag distances can signify big differences in altitude. These gauges potentially show a lot of variance, for example caused by orographic forcing influencing the precipitation amounts. In the case of CSCOMB, this is aggravated by radar problems in complex terrain. Since we assume the same covariance structure everywhere in the domain (stationarity assumption), a nugget induced by the gauges situated in mountainous areas will also cause a lot of small-scale variance in the Swiss Plateau region. This might be in contradiction

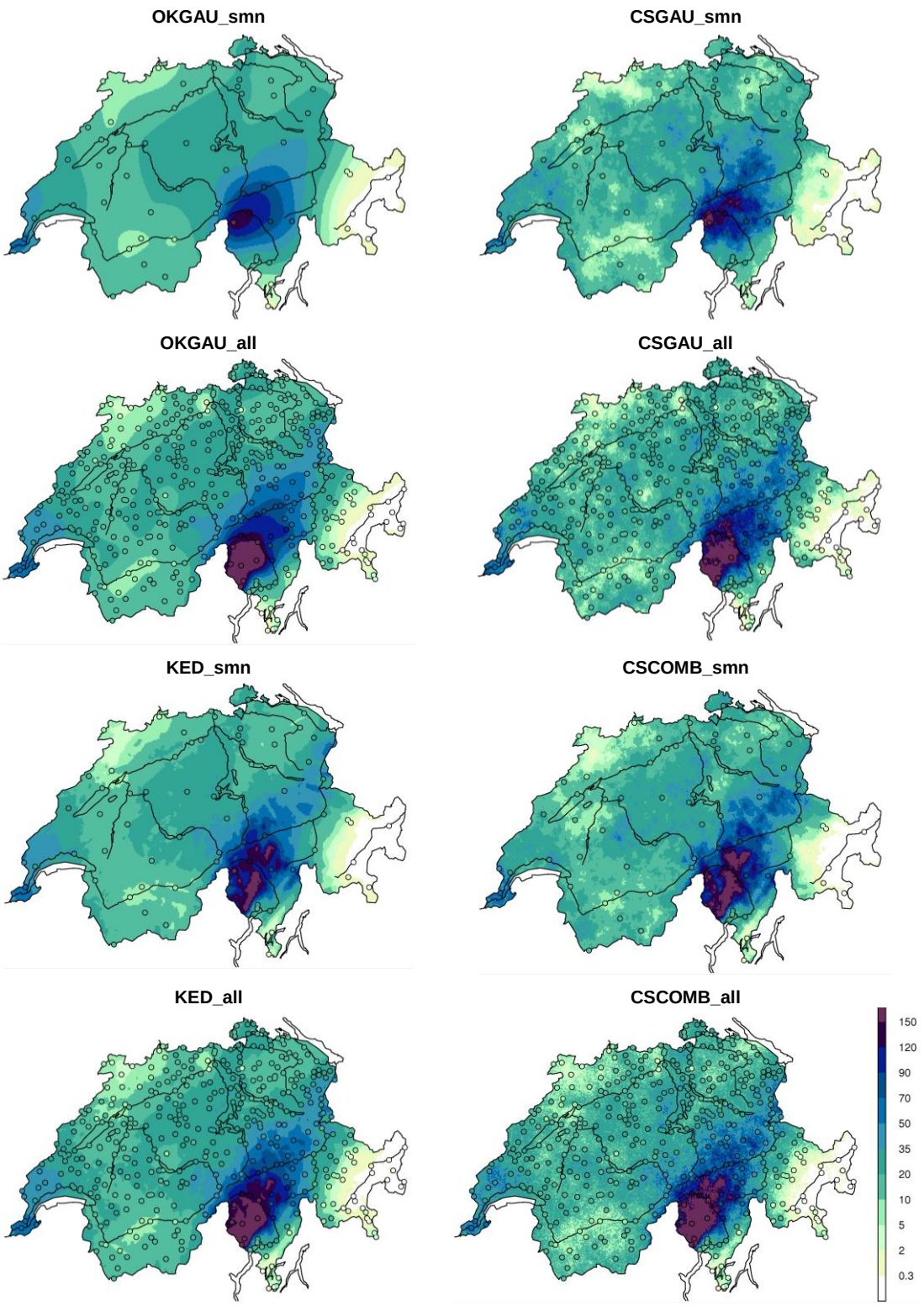

Figure B3 Best estimate fields of precipitation from kriging (left) and one ensemble member from conditional simulation (right) on the 6 September 2008 in mm. Precipitation fields are shown for the single-sensor reference method (OKGAU and CSGAU) and the combination method (KED and CSCOMB) for both network densities.

with the potentially lower variance among the observations in the Swiss Plateau. What we want to stress here is the fact that assuming the same variogram for the entire domain constitutes a considerable simplification of the model. We have to bear this simplification in mind when considering precipitation fields generated with conditional simulation. We should, however, not forget that point values and not areal averages of precipitation are simulated. This approach can enhance small-scale variability.

Also on the 6 September 2008, a better representation of local variability of precipitation is achieved with conditional simulation (Figure B3). Of all the three example days, the 6 September 2008 has the smallest nugget-to-sill ratios when the dense station network is used and a nugget of zero for both CSCOMB_smn and CSGAU_smn. The simulated precipitation fields from conditional simulation therefore have less small-scale variance.

We see the importance of a good sampling for conditional simulation here. With the sparse station network and without using radar information, only one gauge detects the strong precipitation maximum in Ticino. The area of this maximum is therefore much smaller in CSGAU_smn than in CSCOMB or CSGAU_all.

Another interesting issue are the radar artifacts pointing away radially from the Albis radar (we already highlighted these so called radar stripes in section 4.2.6). They are clearly visible in the radar composite (see Figure 2), the best estimate field of KED_smn and the trend field (not shown). Also in the simulated precipitation fields from CSCOMB_smn, the radar stripes are visible. We interpret this as follows: as can be seen in the radar composite, rain gauge measurements and radar information are, with the exception of the southern Valais, in accordance with each other. The good agreement of radar and rain gauge measurements is reflected in the relatively high βs estimated with both station networks (see Figure 2). Residuals at gauges are therefore small and we would expect the influence of the simulated residual field to be limited. Thus, adding the simulated residual fields to the trend cannot remove the radar artifacts present. If we consider the precipitation field from KED_all, we see that the addition of the climatological gauges made the radar stripes become nearly invisible. Using all rain gauge observations available, the network is dense enough to correct the radar artifacts locally. The radar stripes are completely removed in the ensemble members from CSCOMB_all, where the small-scale variance provides further assistance in removing the radar artifacts.

MeteoSchweiz
Krähbühlstrasse 58
CH-8044 Zürich

T +41 44 256 91 11
www.meteoschweiz.ch

MeteoSchweiz
Flugwetterzentrale
CH-8060 Zürich-Flughafen

T +41 43 816 20 10
www.meteoswiss.ch

MeteoSvizzera
Via ai Monti 146
CH-6605 Locarno Monti

T +41 91 756 23 11
www.meteosvizzera.ch

MétéoSuisse
7bis, av. de la Paix
CH-1211 Genève 2

T +41 22 716 28 28
www.meteosuisse.ch

MétéoSuisse
Chemin de l'Aérologie
CH-1530 Payerne

T +41 26 662 62 11
www.meteosuisse.ch